Department of Physics and Astronomy
University of Heidelberg

Bachelor Thesis in Physics
submitted by

Ilya Fokin

born in Kazan (Russian Federation)

2018

Considering the Effects of Radial Flow in Decay Photon Calculations in Ultrarelativistic Nucleus-Nucleus Collisions

This Bachelor Thesis has been carried out by Ilya Fokin at the
Physikalisches Institut in Heidelberg
under the supervision of
Prof. Klaus Reygers

Abstract

In this thesis, three methods for calculating the decay-photon cocktail while taking radial flow into account are compared. This is done by extrapolating the well known spectra of $\pi^{\pm}$ and $K^{\pm}$ to obtain the ones of η, ω and η' mesons, which are the main sources of decay-photons. A cocktail from transverse mass scaling, which does not include radial flow, serves as a baseline. In the first method, the η/π^0 ratio is replaced by the $K^{\pm}/\pi^{\pm}$ ratio due to the similar masses of $K^{\pm}$ and η. This results in 1.05 times more decay-photons in the range between $1\,\mathrm{GeV}$ and $4\,\mathrm{GeV}$. A conclusion of this is that up to 30% of the direct photon spectrum can be attributed to decay-photons. Secondly, a fit with the Tsallis-blastwave model is attempted, but the result does not describe the data. Therefore this model is not suited for extrapolation from this data. Finally, the spectrum is split up into one component that incorporates all radial flow in a blastwave description and one component without radial flow. Similarly to the first method, the decay-photon calculation using this two-component model yields up to 1.05 times more decay-photons. The model was also fit to data from PHENIX. Compared to m_T scaling, the decay photon yield is up to 7% larger which also results in 30% of direct photons attributed to decay-photons.

Kurzzusammenfassung

In dieser Arbeit werden drei Methoden zur Berechnung des Zerfallsphotonencocktails unter Berücksichtigung des radialen Flusses verglichen. Hierzu werden aus bekannten Spektren von $\pi^{\pm}$ und $K^{\pm}$ die Spektren von η, ω und η' Mesonen, die die Hauptquellen von Zerfallsphotonen sind, extrapoliert. Als Vergleichsgrundlage dient ein Cocktail aus m_T scaling, das die radiale Expansion nicht berücksichtigt. In der ersten Methode wird das Verhältnis η/π^0 aufgrund der ähnlichen Massen von $K^{\pm}$ und η durch das Verhältnis $K^{\pm}/\pi^{\pm}$ ersetzt. Dies führt zu 1.05 mal mehr Zerfallsphotonen im Bereich zwischen $1\,\mathrm{GeV}$ und $4\,\mathrm{GeV}$. Daraus lässt sich schließen, dass bis zu 30% des direkten Photonenspektrums auf Zerfallsphotonen zurückzuführen sind. Zweitens wird ein Fit mit dem Tsallis-blastwave Modell versucht, aber das Ergebnis beschreibt die Daten nicht. Daher eignet sich dieses Modell nicht zur Extrapolation aus diesen Daten. Schließlich wird das Spektrum in eine Komponente, die die gesamte radiale Strömung enthält und eine Komponente ohne radiale Strömung aufgeteilt. Wie in der ersten Methode liefert die Zerfallsphotonenberechnung mit diesem Zweikomponentenmodell bis zu 1.05 mal mehr Zerfallsphotonen. Es wird auch ein Fit mit Messwerten der PHENIX Kollaboration durchgeführt. Im Vergleich zur m_T scaling ist die Ausbeute an Zerfallsphotonen um bis zu 7% höher, was ebenfalls zu 30% der direkten Photonen führt, die auf Zerfallsphotonen zurückzuführen sind.

Contents

1 Introduction

Photons are excellent probes to study the system properties in heavy-ion collisions. They are created at every stage of the collision and escape the medium with little interaction since they only interact electromagnetically [1]. The conditions at their creation can be directly studied through measurements of photons. For instance, thermal photons from the thermalized Quark-Gluon Plasma (QGP) and Hadron Gas (HG) can be studied to learn about the thermodynamics of these two stages in the collision. On the other hand, photons from hadron decays, which originate outside the QGP phase, act as a background that has to be subtracted from the total number of measured photons to obtain the spectrum of direct photons. The decay-photon spectrum is usually obtained from Monte Carlo simulations in which hadrons are decayed and the decay products are recorded. For accurate simulations, the momenta of the hadrons have to follow the real momentum distributions, which are often hard to measure. The η, ω and η' mesons together with the π^0 meson account for the vast majority of decay-photons but measurements of the former three particles are not detailed enough to directly obtain their momentum distributions. Instead, the distributions must be extrapolated from measurements of other particles using models. These models should include the collective radial flow of hadrons, which arises from the expansion of the QGP and the HG perpendicular to the beam axis. Because the signal of direct photons above the background of decay-photons is very small, a difference of a few percent in the decay-photon spectrum can change the direct photon measurement by 20 - 30%. Often, m_T scaling, which neglects radial flow, is used to calculate the momentum distributions [2, 3].

In this thesis, different approaches that incorporate radial flow will be used to generate decay-photons. First, the η/π^0 ratio is substituted by the $K^{\pm}/\pi^{\pm}$ ratio because of the similar masses of η and $K^{\pm}$ as well as π^0 and $\pi^{\pm}$. This was partly done by the ALICE collaboration [2]. Secondly, a fit of the Tsallis-blastwave model is attempted, which was previously done by the STAR collaboration [4]. In the third approach the particle spectrum is split into a compontent with and one without radial flow. The two components are then treated separately for the extrapolation to other particles. The results of the decay-photon calculations are compared to a reference calculation that purely uses m_T scaling.

1.1 Kinematic Variables and Observables

In collider experiments, two beams of particles are accelerated to velocities close to the speed of light and then brought to collision in distinct points. In relativistic collisions, the positions and momenta are described using four-vectors [5]:

$$x^\mu = (x^0, x^1, x^2, x^3) = (ct, \mathbf{x}) \tag{1.1}$$
$$p^\mu = (p^0, p^1, p^2, p^3) = (E/c, \mathbf{p}) \tag{1.2}$$

with the position $\mathbf{x}$ in euclidean space, the momentum $\mathbf{p}$, the energy $E = \sqrt{m^2 + \mathbf{p}^2}$ and the speed of light c. From here on, a natural system of units is adopted where $c = \hbar = k_\mathrm{B} = 1$, which is customary in particle physics. This means that mass, energy and momentum have the same dimensions, i.e. $E^2 = m^2 + \mathbf{p}^2$.

After a collision, the collision products are measured in detectors such as ALICE. There are elastic collisions where the total energy of the two particles is conserved and the ingoing particles are equal to the outgoing particles. On the other hand, there are inelastic collisions, in which energy is deposited in the region in which the collision happens. Additional particles can then be created from this deposited energy.

The products of a collision move away from the collision point and are measured by different detectors. The result is the yield or momentum distribution $\frac{\mathrm{d}^3N}{\mathrm{d}^3p}$, which is the number of particles N in a momentum interval $[\mathbf{p}, \mathbf{p} + \mathrm{d}\mathbf{p}]$. Since $\frac{\mathrm{d}N}{\mathrm{d}^3p}$ is not Lorentz invariant, i.e. observers in different inertial frames measure different yields, usually the invariant yield $E\frac{\mathrm{d}^3N}{\mathrm{d}^3p}$ is measured. Because the experiment is rotationally symmetric around the beam axis, the momentum is split into a component along the beam axis, the longitudinal momentum $\mathbf{p}_L$, and one perpendicular to the beam axis, the transverse momentum $\mathbf{p}_T$: $\mathbf{p} = \mathbf{p}_L + \mathbf{p}_T$. Because $\mathbf{p}_T$ is perpendicular to the beam axis, it is also invariant under Lorentz boosts in the direction of the beam axis. The longitudinal momentum is expressed using the rapidity y with $p_L = |\mathbf{p}_L|$:

$$y = \frac{1}{2}\ln\left(\frac{E + p_L}{E - p_L}\right). \tag{1.3}$$

The rapidity changes by an additive constant when the reference frame is Lorentz boosted in the longitudinal direction. As a consequence, the rapidity distribution is shifted by a constant, but the shape is unchanged. Most particles are produced at $y = 0$, or mid-rapidity. In collider experiments with fixed center of mass, this is the direction perpendicular to the beam axis. Higher rapidity indicates a larger longitudinal velocity in this case.

With the transverse momentum and the rapidity, the invariant yield can be written as

$$\begin{aligned} E\frac{\mathrm{d}^3N}{\mathrm{d}^3\mathbf{p}} &= \frac{\mathrm{d}^3N}{p_T\,\mathrm{d}\phi\,\mathrm{d}p_T\,\mathrm{d}y} \\ &= \frac{\mathrm{d}^2N}{2\pi p_T\,\mathrm{d}p_T\,\mathrm{d}y}. \end{aligned} \tag{1.4}$$

where $p_T = |\mathbf{p}_T|$ in the denominator. The invariant yield can also be expressed as a function of the transverse mass $m_T = \sqrt{m^2 + p_T^2}$. The coordinate transformation $p_T \to m_T$ does not change the invariant yield: $\frac{1}{p_T}\frac{\mathrm{d}^2N}{\mathrm{d}p_T\,\mathrm{d}y} = \frac{1}{m_T}\frac{\mathrm{d}^2N}{\mathrm{d}m_T\,\mathrm{d}y}$.

1.2 Heavy-Ion Collisions

At everyday temperatures and energy densities, quarks can only be found in bound states, the hadrons. If the energy density exceeds a few $\mathrm{GeV\,fm^{-3}}$, a phase transition is predicted to occur [6]: similar to the transition in which ice cubes melt into water, the quarks in hadrons become deconfined to form a medium, called the Quark-Gluon-Plasma (QGP).

To achieve an energy density sufficient to create a QGP, two beams of nuclei with large mass numbers A, like lead at the Large Hadron Collider (LHC) ($A_{\mathrm{Pb}} = 208$ [7]) or gold at the Relativistic Heavy-Ion Collider (RHIC) ($A_{\mathrm{Au}} = 197$ [8]) are collided. In inelastic collisions, the kinetic energy of the nuclei is deposited in the central region. The energy density in the central region in heavy-ion collisions is increased compared to proton-proton collisions at similar central of mass energy: there are more nucleon nucleon collisions due to the higher mass number in a small volume. Each of these nucleons can collide with multiple nucleons from the other nucleus, which further increases the energy deposited. Because the nuclei move at a velocity close to the speed of light, they are highly Lorentz-contracted in the lab frame. This means that two colliding nuclei form flat disks instead of spheres in the lab frame, which leads to many nucleon nucleon collisions in a small amount of time and in close proximity [9, p.2]. As the leftovers of the nuclei recede in their respective beam directions, the QGP is formed and thermalizes at about $\tau_0 = 1\,\mathrm{fm}/c$ after secondary scatterings in the collision region. It expands due to the high density gradient between the QGP and the surrounding space and finally cools down. As it cools down, the temperature drops below the chemical freeze-out temperature $T_c \approx 156\,\mathrm{MeV}$ [10] and the system transitions from the QGP phase to a HG. This process is shown in Fig. 1.1.

Due to the large energy density and temperature, the mean free path of particles in the collision is sufficiently small to be described by ideal hydrodynamics [11].

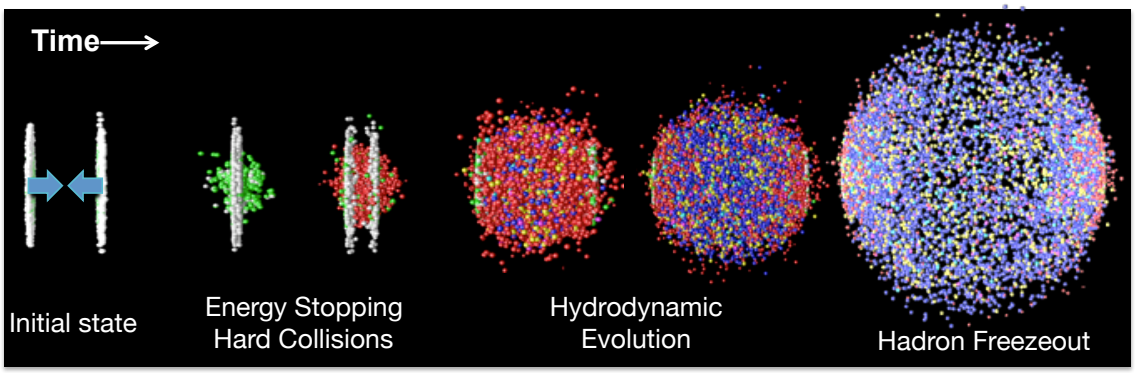

Figure 1.1: Evolution of a heavy-ion collision [12]

Because collective flow arises from the hydrodynamic evolution, it is not sufficient to treat a heavy-ion collision as many separate nucleon-nucleon collisions. One collective effect is the azimutal anisotropy [11]: the overlap of two nuclei colliding in a not exacly central collision with an impact parameter (the distance between the centers of the nuclei in the transverse plane) $b > 0$ is not a circle, but more almond shaped (Fig. 1.2a). Because the hot region is now not isotropic, neither is the pressure gradient which acts on the momentum distribution via hydrodynamical equations of motion. The yield is then not independent of the azimutal angle φ which can be quantified by expanding the yield using Fourier coefficients v_n as

$$\frac{\mathrm{d}N}{\mathrm{d}\varphi} \propto 1 + 2v_1 \cos(\varphi - \Psi) + 2v_2 \cos(2(\varphi - \Psi)) + \cdots \tag{1.5}$$

with the angle $(\varphi - \Psi)$ between the reaction plane, whose orientation can be different for every collision, and the recorded particle (see Fig. 1.2a). The flow parameters v_n depend on p_T and contain information about the collective effects. In particular, v_2 characterizes the amount of elliptic flow.

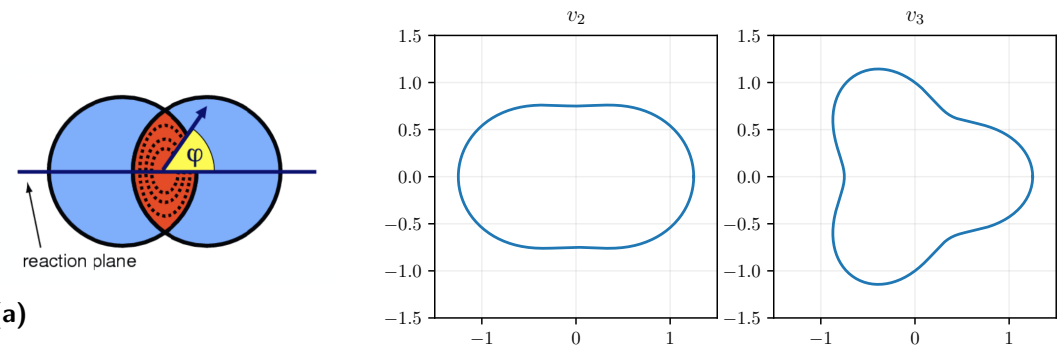

Figure 1.2: a) almond shaped collision region, b) illustration of Fourier coefficients v_2, v_3 in Eq.(1.5)

1.3 A Large Ion Collider Experiment

A Large Ion Collider Experiment (ALICE) [13] is the dedicated heavy-ion collider experiment at the Large Hadron Collider (LHC) [14] at CERN [15]. Its focus lies on the study of the strong interaction in the Standard Model. It was designed to measure large charged particle multiplicities of up to $\mathrm{d}N_{\mathrm{ch}}/\,\mathrm{d}y \approx 8000$ in heavy-ion collisions with good particle indentification using multiple separate detectors. Tracking and particle identification is done by the Inner Tracking System (ITS) and Time-Projection Chamber (TPC) near the beam axis e.g. by the specific energy loss $\mathrm{d}E/\,\mathrm{d}x$.

Photons can be reconstructed using the Photon Conversion Method by measuring the tracks of electron-positron pairs from $\gamma + Z \rightarrow e^+ + e^- + Z$ with the TPC or the ITS [2]. Alternatively, the photons can be measured directly by the two electromagnetic calorimeters, the PHOton Spectrometer (PHOS) and the ElectroMagnetic Calorimeter, EMCal. PHOS is designed to measure photons at low p_T such as thermal photons while EMCal has a worse energy resolution, but can measure photons at high p_T.

1.4 Photons as Electromagnetic Probes

Since quarks are deconfined in the QGP, the bound states of quarks, hadrons, are only produced at the freeze-out surface, which is the boundary between the hot QGP and the cold surrounding space [16]. This is similar to hot water in a closed container: at the water surface, the vapour always condenses with a temperature of $100\,^{\circ}\mathrm{C}$ at a pressure of $1\,\mathrm{atm}$, giving no information about the vapour further away from the water surface. Photons, on the other hand, are also produced in the QGP and the HG at all stages of the collision for example in π^+-π^- annihiliation ($\pi^+ + \pi^- \rightarrow \rho^0 + \gamma$) in the HG or in quark-antiquark annihilation ($q + \bar{q} \rightarrow g + \gamma$) or quark-gluon Compton scattering ($q + g \rightarrow q + \gamma$) in the QGP [17].

The production rate and momentum distribution of photons from the two latter reactions depend on the momentum distributions of the quarks and gluons and thus also on the thermodynamical state of the QGP. Because photons only interact via the electromagnetic interaction, their mean free path is larger than the fireball and they escape the medium unscathed after they are created. They then also contain information about every stage of the collision, not only about the freeze-out surface of the QGP.

There are multiple sources of photons in a heavy-ion collision such as the thermal radiation of the QGP itself, the thermal radiation of the HG after the freeze-out and decays of other particles into photons such as $\pi^0 \rightarrow \gamma\gamma$. Photons from particle decays (decay-photons γ_{dec}) make up the vast majority of the measured inclusive photon yield $\gamma_{\mathrm{inc}} = \gamma_{\mathrm{dir}} + \gamma_{\mathrm{dec}}$, but they contain little information about the QGP as they are produced from hadron decays. The photons that do not originate from decays are called direct photons γ_{dir}. The decay-photon yield acts as a background to the signal of direct photons and has to be subtracted from

the direct photon yield. $\gamma_{\rm dec}$ can be obtained in Monte Carlo simulations where various hadrons are decayed and the produced photons are recorded [2, 3]. This is also called the decay-photon cocktail simulation because there are many '*ingredients*' (photons from many different hadrons) that make up the spectrum. For the Monte Carlo simulation, the momentum distributions of the to-be-decayed hadrons are crucial as the momentum distributions of decay products depend on the ones of the mother particles. In case of the η, ω and η' mesons, where only little data is available , the momentum distributions must be extrapolated from available data of other particles. In this thesis, different approaches for this will be carried out and compared.

In practice, the direct photon excess is characterized by the double ratio

$$R_\gamma = \frac{\gamma_{\rm inc}/\pi^0}{\gamma_{\rm dec}/\pi^0} = \frac{\gamma_{\rm inc}}{\gamma_{\rm dec}} = \frac{\gamma_{\rm dec}+\gamma_{\rm dir}}{\gamma_{\rm dec}} = 1 + \frac{\gamma_{\rm dir}}{\gamma_{\rm dec}} \tag{1.6}$$

because the division by the π^0 spectrum in the enumerator and denominator cancels out some of the systematic uncertainties [2]. A double ratio $R_\gamma > 1$ indicates a direct-photon signal which becomes smaller as R_γ approaches 1. The direct photon yield is then retrieved using

$$\gamma_{\rm dir} = \gamma_{\rm inc} - \gamma_{\rm dec} = \left(1 - \frac{1}{R_\gamma}\right)\gamma_{\rm inc}. \tag{1.7}$$

In measurements [2, 3], R_γ was ≈1.1-1.3 for the most central collisions at low p_T. In this thesis, the decay-photon yield $\gamma_{\rm dec}$ will be calculated in different scenarios which changes R_γ in Eq.(1.6). Since the inclusive photon spectrum is measured, only $\gamma_{\rm dec}$ in the denominator is modified. An increased decay-photon yield $\widetilde{\gamma}_{\rm dec} = (1+\epsilon)\gamma_{\rm dec}$ results in

$$\widetilde{R}_\gamma = \frac{\gamma_{\rm dec}+\gamma_{\rm dir}}{\widetilde{\gamma}_{\rm dec}} = \frac{\gamma_{\rm dec}+\gamma_{\rm dir}}{(1+\epsilon)\gamma_{\rm dec}} = \frac{R_\gamma}{1+\epsilon} \tag{1.8}$$

Not only the yield of direct photons can be measured, but also their elliptic flow coefficient v_2. When comparing the direct photon yields and the direct photon v_2 to predictions from models, it was noticed [18] that the theory cannot describe the two quantities simultaneously in measurements at RHIC. This is shown in Fig. 1.3 and has been dubbed the 'direct photon flow puzzle' [19] or 'photon flow puzzle' [18]. In ALICE measurements, this discrepancy is much smaller [20].

Furthermore, the results from the STAR collaboration are much closer to the theory than the ones from the PHENIX collaboration even though the measurements were both done at RHIC and should be therefore similar. One difference between these two measurements is the method to obtain the unknown momentum distributions of hadrons for the decay-photon simulaton: while the PHENIX collaboration used m_T scaling (1.5), the STAR collaboration used Tsallis-blastwave fits (1.7)

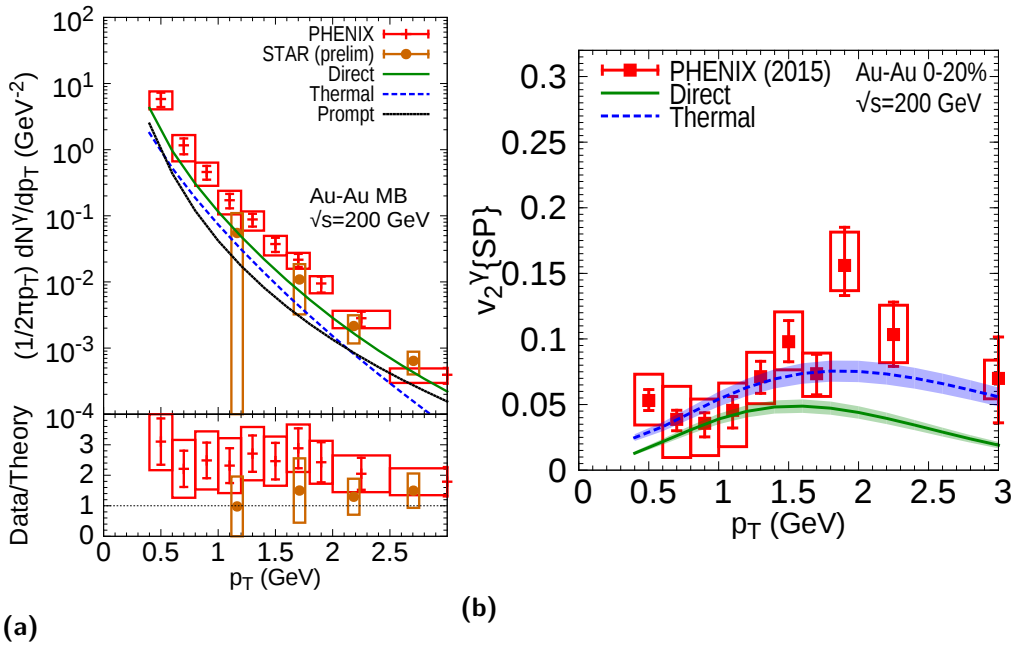

Figure 1.3: Direct photon flow puzzle: a) direct photon invariant yield, b) direct photon v_2

1.5 Transverse Mass Scaling

It has been observed [21, 22] that the invariant yields of many particles as functions of the transverse mass

$$m_T = \sqrt{p_T^2 + m^2} \tag{1.9}$$

can be described by a universal function u of the transverse mass:

$$\frac{\mathrm{d}N}{p_T\,\mathrm{d}p_T} = C_X u(m_T) \tag{1.10}$$

This behaviour is called transverse mass- or m_T scaling. A parametrization of a well known spectrum like the one of charged pions ,f^π, can be used to obtain the invariant yield of a particle X with mass m_X, f^X:

$$f^X(p_T) = C_X f^\pi\left(\sqrt{p_T^2 + m_X^2 - m_\pi^2}\right) \tag{1.11}$$

with m_T scaling factors C_X. These factors are usually obtained in experiments by measuring the ratio X/π^0 at high p_T or by simulating proton-proton collisions and measuring the particle ratios at high p_T [19].

m_T scaling is commonly used to predict the invariant yields of particles for which there is little data for use in decay-photon yield calculations [23, 3]. In Au+Au collisions, deviations from m_T scaling have been attributed to the presence of radial flow [24].

1.6 Blastwave Model

One attempt to describe invariant yields from collisions with radial flow is provided in Ref. [25]. The authors start out with the invariant spectrum of particles from a stationary source with uniform temperature T, which follows a Boltzmann distribution:

$$\frac{\mathrm{d}^3N}{\mathrm{d}y\,\mathrm{d}\phi\,m_T\,\mathrm{d}m_T} \propto E\exp\left(-E/T\right) \tag{1.12}$$

To account for transverse flow, a radial velocity profile $\beta_r(r)$ for radii up to the surface of the fireball with radius R is assumed:

$$\beta_r(r) = \beta_s\left(\frac{r}{R}\right)^n \tag{1.13}$$

with the velocity at the surface of the expanding medium β_s and the exponent n which determines the shape of the profile. The individual thermal sources are now Lorentz-boosted according to their velocity $\beta_r(r)$ and rapidity y. The particles emitted by the boosted sources have, on average, higher momenta than the ones from stationary sources, which increases the invariant yield at higher p_T. The boost is larger for heavier particles than for light ones [26]. The resulting spectrum after boosting and integrating over ϕ and y is:

$$\frac{\mathrm{d}N}{m_T\,\mathrm{d}m_T} \propto \int_0^R r\;\mathrm{d}r\,m_T\,I_0\left(\frac{p_T\sinh\rho}{T}\right)K_1\left(\frac{m_T\cosh\rho}{T}\right) \tag{1.14}$$

with $\rho = \tanh^{-1}(\beta_r(r))$ and I_0, K_1 modified Bessel functions of first and second kind. For stationary sources, i.e. $\beta_r = 0$, $I_0(...) = 1$ and Eq.(1.14) only depends on m_T, which means that m_T scaling becomes applicable. Therefore, a deviation from m_T scaling can be seen as a sign for collective flow [27]. The free parameters in Eq.(1.14) are n, β_s, T as well as the normalization.

Eq.(1.12) describes only the primary hadrons, not the decay products of other hadrons. This 'feeddown' from heavy to lighter particles has to be considered when using Eq.(1.14) to describe measurements.

1.7 Tsallis-Blastwave Model

The Tsallis distribution generalizes the Boltzmann distribution by introducing a parameter q, which describes the degree of non-equilibrium in the emitting source. With the Tsallis distribution, the invariant yield becomes

$$\frac{\mathrm{d}^2N}{\mathrm{d}y\, m_T\, \mathrm{d}m_T} \propto \left(1 + \frac{q-1}{T}\, m_T\right)^{-1/(q-1)}. \tag{1.15}$$

For $q \to 1$ and $m_T = E$ for $y = 0$, this reduces to the Boltzmann distribution in Eq.(1.12). Applying the same procedure as before, the authors in Ref. [28] arrive at

$$\begin{aligned}\frac{dN}{m_T dm_T} \propto m_T \int_{-Y}^{+Y} \cosh y dy \int_{-\pi}^{+\pi} d\phi \int_0^R r dr \\ \left(1 + \frac{q-1}{T}\left(m_T \cosh y \cosh\rho - p_T \sinh\rho \cos\phi\right)\right)^{-1/(q-1)}\end{aligned} \tag{1.16}$$

with a velocity profile $\beta_r(r)$ and ρ like before. This $[-Y, +Y]$ is a small interval around zero. The largest contribution comes from particles with rapidities $y \approx 0$. Therefore integration in some rapidity interval $[-Y, +Y]$ is enough to get a good approximation for the integral over all rapidities in $(-\infty, +\infty)$.

Baseline: Transverse Mass Scaling

2

To judge the particle cocktail and to see the effects of the different methods on the particle composition, a reference cocktail is needed. As ALICE and PHENIX at least partly use m_T scaling for the prediction of the spectra, the reference is also calculated by extrapolating a parametrization of the π^0 yield to other particles using m_T scaling.

2.1 Neutral Pion Parametrization

The π^0 parametrization is obtained by a fit to the invariant yield in Ref. [29] with the two-component model described in Chapter 5 (Eq.(5.3)) instead of the given parametrization in the paper. The new parametrization does not increase as steeply for $p_T \to 0$ and therefore gives reasonable particle ratios for low p_T instead of ratios very close to zero, which would give rise to artifacts in the cocktail generation. The fit and parameters are shown in Appendix 7.2.

2.2 Cocktail Generation

For the cocktail generation, a *ROOT* [30] script by [31] was used and extended to include other methods of obtaining X/π^0 ratios for other hadrons X. The script takes as input a parametrization of the neutral pion spectrum $(\mathrm{d}N/\,\mathrm{d}p_T)_{\pi^0}$ as well as parametrizations of the particle ratios $(dN/dp_T)_X \,/\, (dN/dp_T)_{\pi^0}$. A list of hadrons, which should be decayed, has to be specified as well. Previous cocktail calculations (see Fig. 2.1, [19]) showed that the contributions from π^0, η, ω and η' mesons make up most of the decay-photon yield. About 80% of decay-photons originate from π^0 decays. The second largest contribution ($\approx 10-15\%$) comes from decays of η mesons. Photons from ω meson decays make up about 2% and the ones from η' make up less than 1% of the total decay-photon yield. Decays of other particles contribute less than 0.1%.

Because of this and in order to speed up the computation, only these four particles are considered here. In the main loop of the cocktail generator, p_T, ϕ and the rapidity y are sampled from a uniform distribution at each iteration. p_T ranges from 0 to $30\,\mathrm{GeV}$, ϕ from 0 to 2π and y from -1.5 to 1.5. One of each of the four mesons is generated with the sampled kinematic variables. Each of the particles is assigned a weight

$$w_X(p_T) = (\mathrm{d}N/\,\mathrm{d}p_T)_{\pi^0} \frac{(\mathrm{d}N/\,\mathrm{d}p_T)_X}{(\mathrm{d}N/\,\mathrm{d}p_T)_{\pi^0}}. \tag{2.1}$$

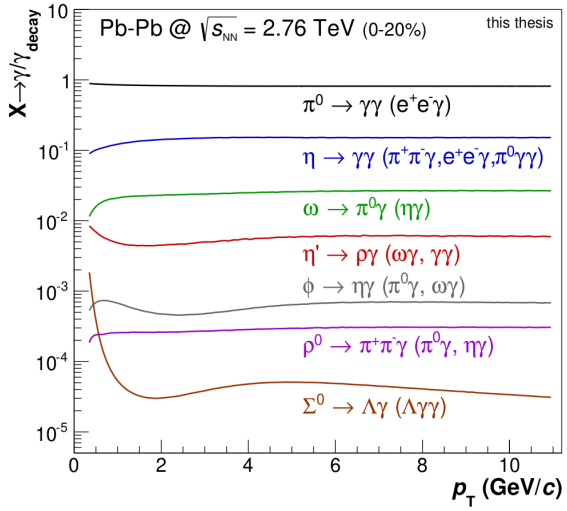

Figure 2.1: Contributions to decay-photon cocktail, calculated in [19]

Using the weights instead of sampling p_T directly from the momentum distribution $(\mathrm{d}N/\,\mathrm{d}p_T)_{\pi^0}$ speeds up the generation considerably: the particle yields at momenta close to zero are many orders of magnitude larger than those at for example $8\,\mathrm{GeV}$ (see Fig. 5.1). For every particle at low p_T, one would on average have to generate on the order of 10^4 particles to get photons from hadrons with $p_T > 5\,\mathrm{GeV}$. With weights, the whole p_T range can be sampled quickly and accurately.

In the next step, the mesons are decayed into other particles using the *PYTHIA8* [32] decayer. The photons resulting from the decays are then written into separate histograms for each particle species with the weights from above.

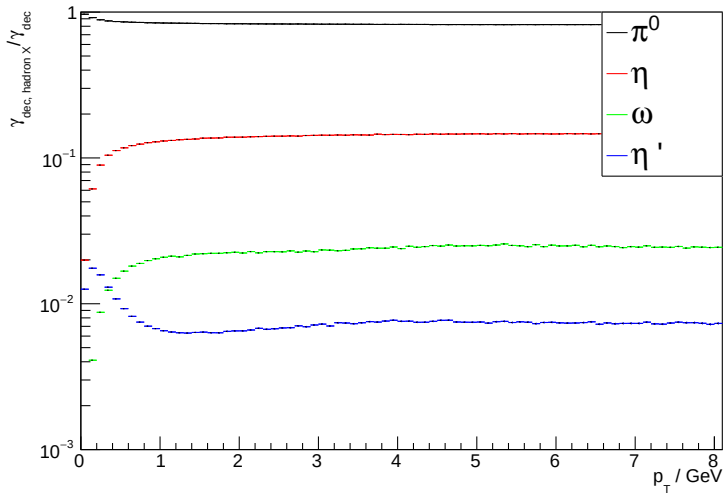

Figure 2.2: Reference cocktail using m_T scaling

For visualization, the photon yields are split up according to the particle species that they originated from and then divided by the sum of all photons to show how much they

contribute to the overall yield in Fig. 2.2. This baseline cocktail of the four most relevant particles is similar to the one in Fig. 2.1. The m_T scaling factors are $C_\eta = 0.46$, $C_\omega = 0.81$ and $C_{\eta'} = 0.4$ [19].

3 Kaon-Pion Ratio as Approximation

3.1 Description

The previous cocktail calculation showed that the contribution of η mesons to the decay-photon cocktail is the second largest after the one from π^0. Because measurements of π^0 spectra [29, 33] are detailed enough to be directly parametrized, the spectrum of the η meson is the most important one to predict accurately. In contrast to the η meson, the charged kaons $K^{\pm}$ are abundant and more easily measured in heavy-ion collisions. Due to their similar masses ($m_\eta = 547.9\,\mathrm{MeV}$, $m_{K^\pm} = 493.7\,\mathrm{MeV}$ [34]), it is assumed that their invariant yields have similar shapes and that they are similarly affected by radial flow. This opens up the possibility to use the well measured kaon spectrum and its ratio to the pion yield in place of the η spectrum for which there is much less data available. Via the same reasoning, the π^0 yield is also replaced by the yield of the charged pions $\pi^{\pm}$ as their masses are almost identical: $m_{\pi^0} = 135.0\,\mathrm{MeV}$, $m_{\pi^\pm} = 139.6\,\mathrm{MeV}$ [34].

For this, the invariant yields for $\pi^{\pm}$ and $K^{\pm}$ are taken from [23] for 0-20% centrality in order to compare the results to the R_γ in Ref. [2]. Dividing the invariant yields then gives the $K^{\pm}/\pi^{\pm}$ ratio that is needed for the cocktail generator. In order to get a parametrization of the ratio, a fit is done with the quotient of two functions of the form

$$\left(\frac{\mathrm{d}N}{p_T\,\mathrm{d}p_T}\right)_X(p_T) = N_1 \exp\left(\frac{\beta p_T - \sqrt{p_T^2 + m_X^2}}{T_{\mathrm{kin}}\sqrt{1-\beta^2}}\right) + C_X N_2 \left(1 + \frac{p_T^2}{p_0^2}\right)^{-n} \tag{3.1}$$

where N_1, N_2 are normalizations, T_{kin} is the kinetic freezeout temperature, β is a flow velocity, m_X is the particle mass, C_X is the m_T scaling factor for particle X and p_0 and n are parameters for the Hagedorn term. For kaons and pions, the corresponding masses are fixed and $C_\pi = 1$ is set because the invariant pion yield is the reference for all particles. C_K is given by the best fit and all other parameters are common for the enumerator and denominator functions.

Because the $K^{\pm}/\pi^{\pm}$ ratio is used immediately as the η/π^0 ratio, the analytic form of the parametrization is not important as long as the fit describes the data reasonably well.

The measured ratios and and the best fit is plotted in Fig. 3.1. For comparison, the ratio obtained from m_T scaling the invariant π^0 yield f^π using

$$\frac{K^{\pm}}{\pi^{\pm}} = C_K \frac{f^{\pi}\left(\sqrt{p_T^2 + m_K^2 - m_{\pi}^2}\right)}{f^{\pi}\left(p_T\right)} \tag{3.2}$$

is also shown in Fig. 3.1. As was already seen in Ref. [23], the kaon-to-pion ratio shows a distinct peak around $p_T \approx 2 - 3\,\mathrm{GeV}$ which is reflected in the parametrization. The ratio from m_T scaling on the other hand does not show this feature. Because of this, the ratio at $\approx 2.5\,\mathrm{GeV}$ is about 30% larger in the new model than it is with m_T scaling.

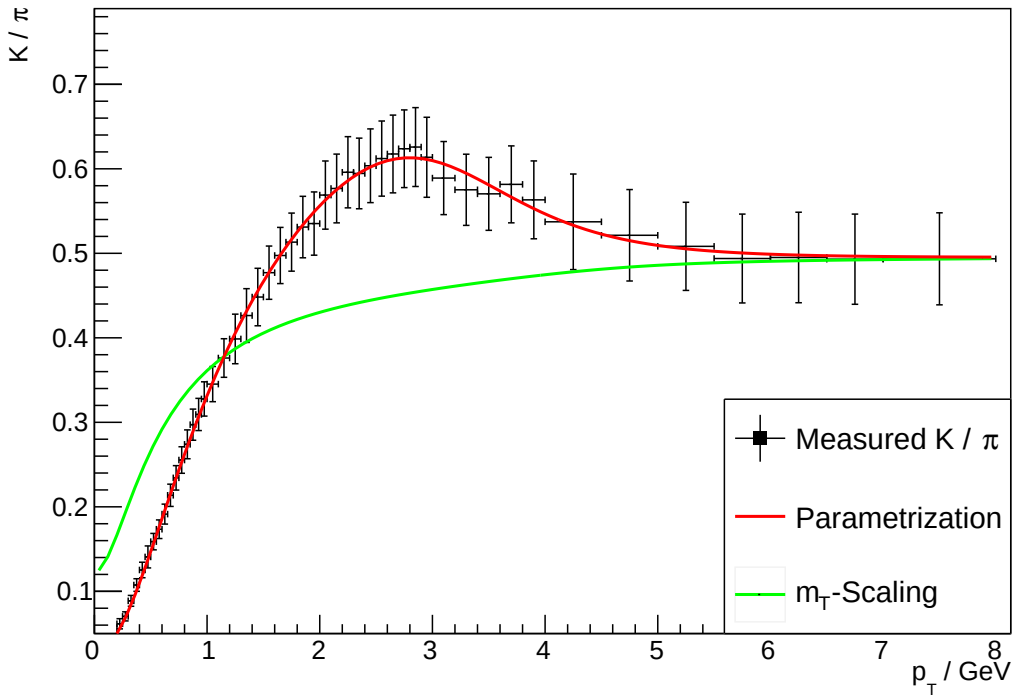

Figure 3.1: $K^{\pm}/\pi^{\pm}$ ratio with best fit (Eq.(3.1)) and ratio from m_T scaling for comparison

To be consistent with measured η/π ratios at high p_T, the m_T scaling factor of the η meson ($C_\eta = 0.46$ [33]) is used in the cocktail generator instead of the one for kaons.

3.2 Cocktail Simulation

With this η/π^0 ratio, the cocktail generator is run for 10^8 particles. For every meson, the decay-photon yield from this model is divided by the yield from the reference cocktail that uses m_T scaling and plotted in Fig. 3.2a. Because only the η meson yield is modified here, the yields from other hadrons are unchanged. The photon yield from η mesons increases at $1 - 4\,\mathrm{GeV}$ because of the increased η/π^0 ratio in Fig. 3.1. At $2\,\mathrm{GeV}$, the number of photons from η decays increases to ≈1.35 times the reference yield. Because photons from η decays account for ≈15% of all decay-photons, this increases the decay-photon yield γ_{dec} by 5% compared to the reference as seen in Fig. 3.2b.

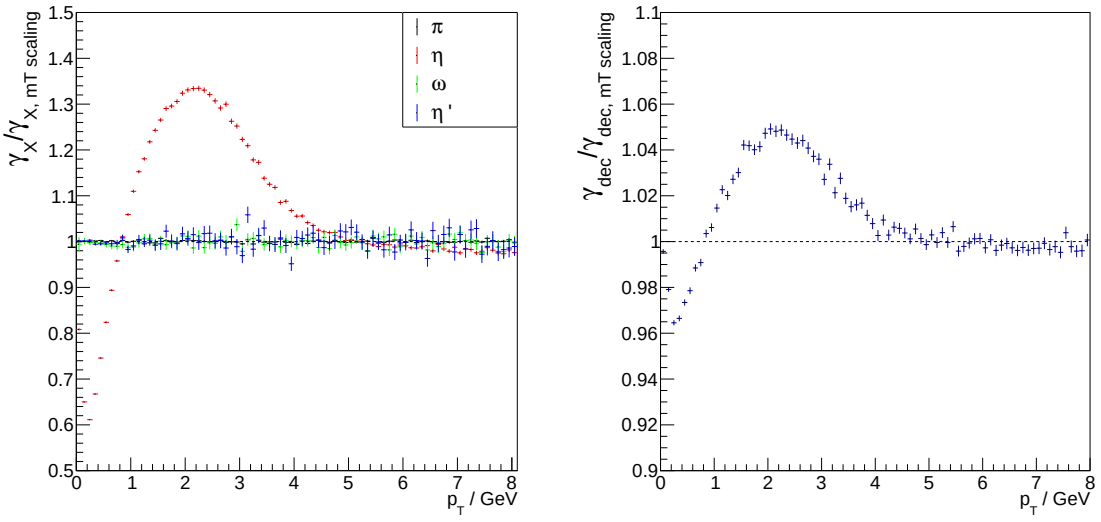

(a) **(b)**

Figure 3.2: Ratio of decay-photon yield from $K^{\pm}/\pi^{\pm}$ ratio to the one from m_T scaling. (a) by particle species, (b) in total

This change affects the direct photon excess R_γ as shown in Section 1.4. R_γ was measured at ALICE and published in Ref. [2] and is shown in Fig. 3.3 for the 0-20% centrality class. The measured R_γ for $\approx 2\,\mathrm{GeV}$ is ≈1.1. In Ref. [2] the average of m_T scaling and the ratio of K^0_S to π^0 was used. Because the K^0_S has a mass of $497.6\,\mathrm{MeV}$ [34], the $K^0_S/\pi^{\pm}$ ratio should have approximately the same shape as the $K^{\pm}/\pi^{\pm}$ ratio. To check this qualitatively, the K^0_S yield for $\sqrt{s_{\mathrm{NN}}} = 2.76\,\mathrm{TeV}$ is taken from [35]. The measurements of K^0_S and $\pi^{\pm}$ have different binnings and it is therefore not possible to directly calculate the $K^0_S/\pi^{\pm}$ ratio on every data point. The $\pi^{\pm}$, $K^{\pm}$ and K^0_S invariant spectra therefore are linearly interpolated (i.e. the points are connected by straight lines) and the ratios are calculated using the interpolation. One side effect of this are artifacts in the plot at higher p_T: at high momenta, the bins are much wider than at low momenta. In the middle of the wide bins, the interpolation does not describe the data well and a new data point in the enumerator (the kaon spectrum) or the denominator (the pion spectrum) creates a large kink in the curve. At low p_T, the momentum bins are much smaller and the kinks are less noticeable. For easier comparison, the K^0_S yield is multiplied by a constant such that the ratios are equal at high p_T and both ratios are plotted in Fig. 3.4. The peak that is clearly visible in the $K^{\pm}/\pi^{\pm}$ ratio seems to be much smaller for K^0_S mesons although one would expect the momentum distributions to look very similar if the shape mostly depends on the mass.

Because the average of the cocktail calculations from m_T scaling and the ratio from K^0_S was used in Ref. [2], less than half of the increase in decay-photons from Fig. 3.2b is accounted for. If the decay-photon yield at $p_T = 2\,\mathrm{GeV}$ was 3% higher than the one used in Ref. [2], the photon excess R_γ would go down from ≈1.1 to ≈1.07. In other words, $R_\gamma - 1 = \gamma_{\mathrm{dir}}/\gamma_{\mathrm{dec}}$ decreases from ≈0.10 to ≈0.07. The direct photon yield would thus decrease by about 30%.

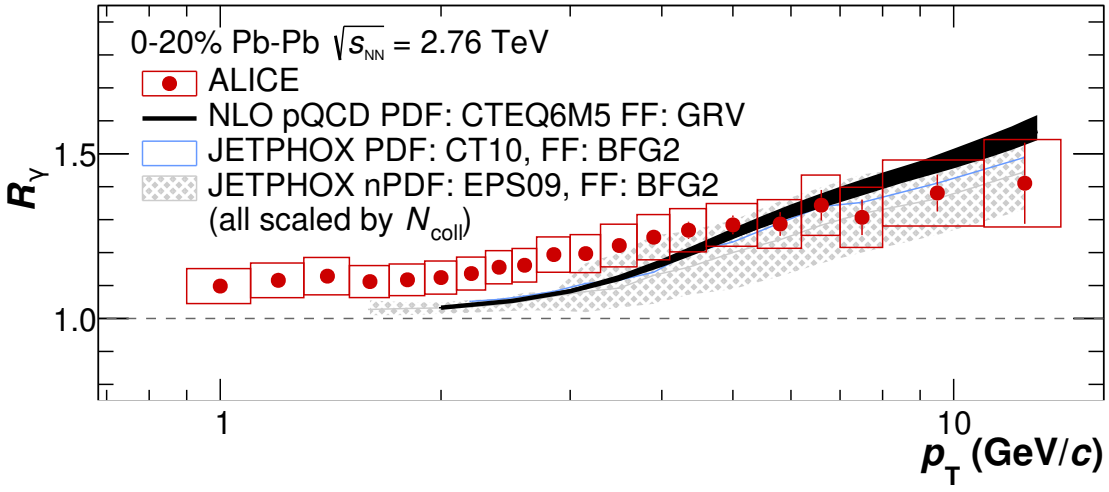

Figure 3.3: Direct photon excess R_γ at ALICE [2]

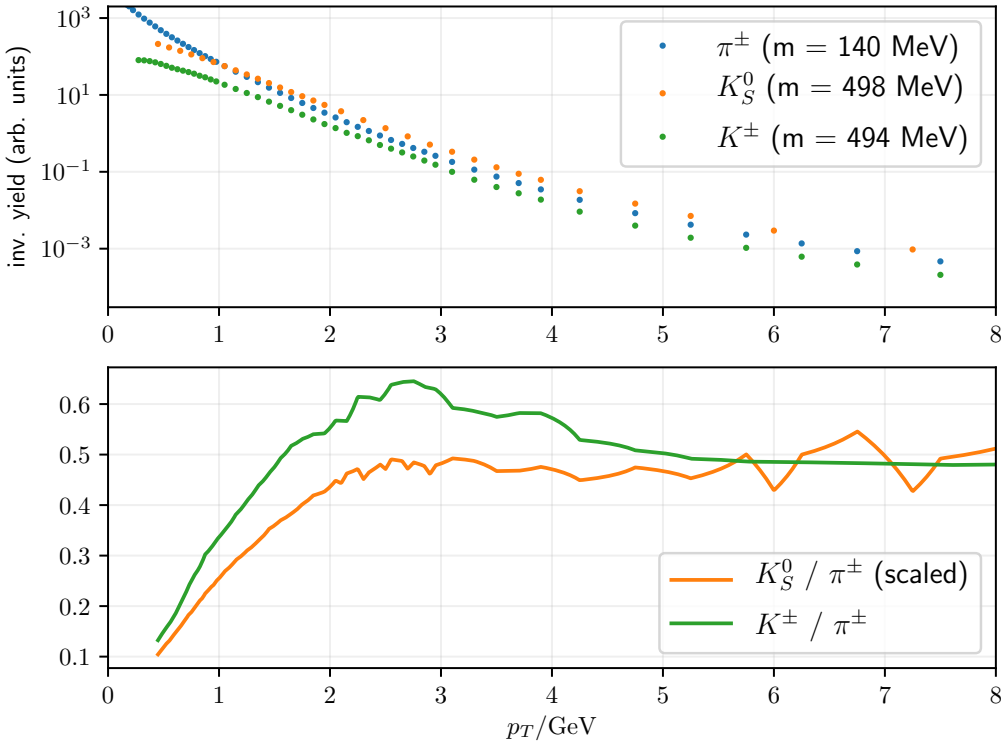

Figure 3.4: Comparison of $K^0_S/\pi^\pm$ and $K^\pm/\pi^\pm$

Tsallis-Blastwave Fits

4

The procedure to predict unknown particle yields using a Tsallis-blastwave model (Chapter 1.7) is as follows: First, the function for the invariant yield (Eq.(4.1)) from the model is fit to measured spectra for various particles. For different particle species, the mass and normalization are different, all other parameters are common for all particles.

$$\begin{aligned}\frac{dN}{p_T dp_T} =& A\, m_T \int_{-Y}^{+Y} \cosh y dy \int_{-\pi}^{+\pi} d\phi \int_0^R r dr \\ & \left(1 + \frac{q-1}{T}\left(m_T \cosh y \cosh \rho - p_T \sinh \rho \cos \phi\right)\right)^{-1/(q-1)}\end{aligned} \tag{4.1}$$

After obtaining the parameters, the unknown yields are predicted by replacing the mass in Eq.(4.1) by the mass of the desired particle. This yield is then divided by the yield for π^0 from this same model. The ratio is then scaled such that it matches the measured ratio X/π^0 at $p_T = 5\,\mathrm{GeV}$. With this ratio, a cocktail generation can then be done.

In [28], the authors find that the mesons and baryons form two separate groups with two sets of common best fit parameters. Therefore, it makes sense to only fit mesons as the four particles whose decay products constitute the vast majority of the decay photon yield, the π^0, η, ω and η', are all mesons. The most readily available measurements of mesons are those of $\pi^{\pm}$ and $K^{\pm}$. To these yields from ALICE [23], a fit is done and plotted in Fig. 4.1.

The fit did not converge to a reasonable result over the whole region. The fit range was then adjusted to give a good $\chi^2/\mathrm{d.o.f.}$ while taking as much of the data into account as possible. Outside of the range $1\,\mathrm{GeV} < p_T < 4.5\,\mathrm{GeV}$, the fit does not describe the data anymore. This is clearly a problem as matching at $5\,\mathrm{GeV}$ is not possible now. The data / fit plot in Fig. 4.1b also shows that even in the fit range where the data is relatively close to the fit, the yield of the kaons is mostly larger than the fit and the one of pions is equal or slighty smaller. In Fig. 4.2, the ratio of the functions in Fig. 4.1a is shown together with the data. The ratio should closely resemble the data, but the plot shows that this fit barely describes the data in the fit range and does not describe the data at all outside of the fit range. Doing a cocktail simulation with particle ratios derived from this fit would not give realistic results. If the prediction of known particle momentum distributions does not follow the data there is no reason to assume that the predictions of particle yields of unknown particles are anywhere close to the real yields.

The model can not describe the bump in the $K^{\pm}/\pi^{\pm}$ should not be used for decay-photon calculations. To incorporate flow for particles other than the η, another method is necessary.

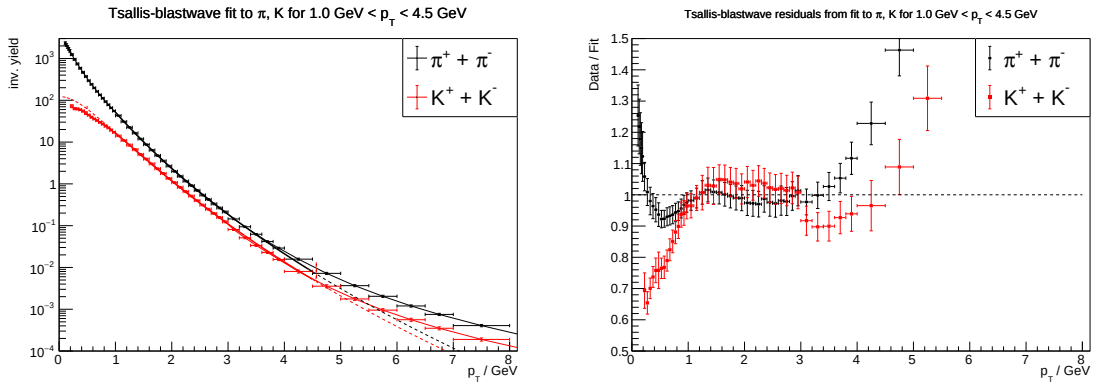

(a) **(b)**

Figure 4.1: Simultaneous fit to $\pi^{\pm}$ and $K^{\pm}$ invariant yields using Tsallis-blastwave model. (a) data with best fit functions, (b) data / fit

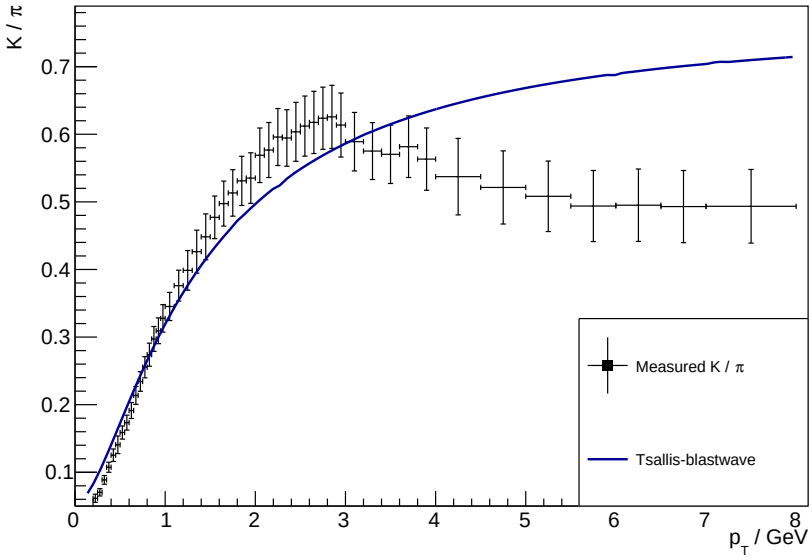

Figure 4.2: Measured $K^{\pm}/\pi^{\pm}$ ratio with ratio of the fit functions from Fig. 4.1

Two Component Model

5

5.1 Description of the Model

Another approach is to split the invariant yield into one soft component, f_{soft}, for low p_T with radial flow and one hard component, f_{hard}, for high p_T without radial flow: $f(p_T) = f_{\text{soft}}(p_T) + f_{\text{hard}}(p_T)$ [31]. For the soft component, the blastwave model from Eq.(1.14) is used. For the hard component, the chosen parametrization is the sum of two Hagedorn-type terms

$$f_{\text{hard}}(p_T) = A_1 \left(1 + \frac{m_T}{p_1}\right)^{-n_1} + A_2 \left(1 + \frac{m_T}{p_2}\right)^{-n_2} \tag{5.1}$$

The exact form of the f_{hard} is not crucial as long as it describes the data since m_T scaling is used as an empirical observation. Other spectral shapes such as $A\left(1 + m_T/p_0\right)^{-n}$ or $A\left(1 + m_T^2/p_0^2\right)^{-n}$ resulted in worse fits which is why the above form was used. To illustrate the two-component model, the sum is fit to the invariant yield of charged pions from [23] and the components are plotted separately with the parameters obtained from the fit in Fig. 5.1. In addition, the fraction of the soft and hard component with respect to the sum are shown in Fig. 5.2. One can see that for low p_T (below $1\,\text{GeV}$), the soft component dominates. At $p_T \to 0\,\text{GeV}$, the soft components comprises 90% of the spectrum. For high p_T (above $\approx 4\,\text{GeV}$) the contribution from the soft component drops to many orders of magnitude below that of the hard component.

After obtaining the parameters (normalization of the pion spectrum, β_s, T and n) for the blastwave model (e.g. from a fit to the pion yield), unknown spectra can be predicted by replacing the mass and multiplying the normalization by the factor A_X such that the ratios of particle densities match the ones predicted from the statistical model (Appendix 7.1):

$$A_X := \frac{N_X}{N_\pi} \approx \frac{m_\pi^2 K_2(m_\pi/T_{\text{kin}})}{m_X^2 K_2(m_X/T_{\text{kin}})} \frac{m_X^2 K_2(m_X/T_{\text{chem}})}{m_\pi^2 K_2(m_\pi/T_{\text{chem}})} \tag{5.2}$$

T_{kin} and T_{chem} are the kinetic and chemical freeze-out temperatures. After the fireball cools down below T_{chem}, the inelastic collisions cease and the particle composition becomes fixed. When it cools down below T_{kin}, elastic collisions stop and the momentum distributions are fixed [36]. T_{chem} has been determined to be $156\,\text{MeV}$ [10] and T_{kin} is the fit parameter in the blastwave model.

The statistical model describes the amount of primary particles produced in the collision, but not the measured particle yields which also include decay products. This process,

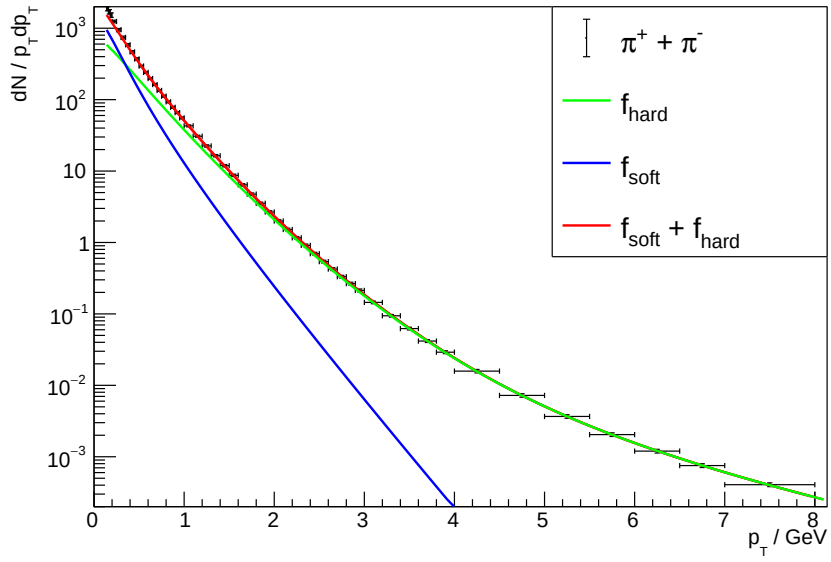

Figure 5.1: Two component fit to charged pions with soft and hard components separated

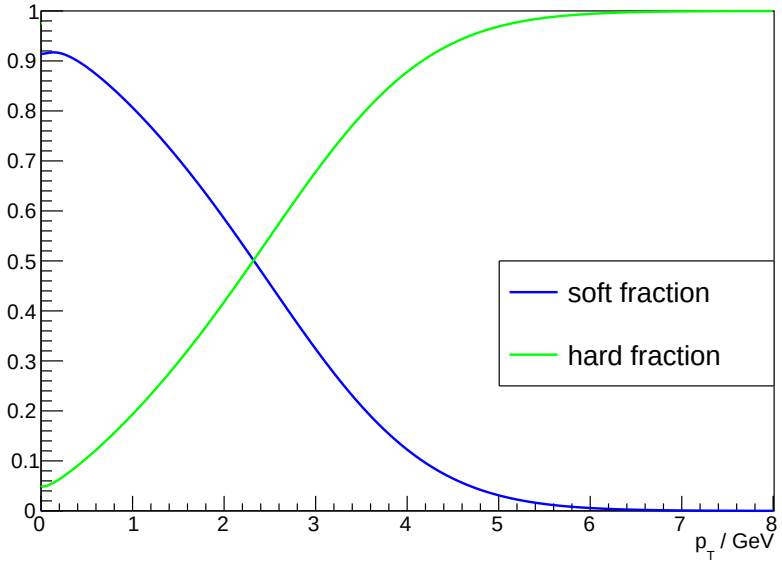

Figure 5.2: Fraction of soft and hard components from fit to charged pions

in which heavy particles contribute to the yields of lighter particles by decays, is called feeddown. Feeddown can be simulated by creating primary particles of many different species with momentum distributions discribed by the blastwave model in Eq.(1.14) and letting them decay e.g. using *PYTHIA8*. One can then calculate the fraction of primary particles to primary + secondary particles. This fraction is approximately constant and the ratio of primary fractions of a hadron X to the one of neutral pions seems to be approximately the m_T scaling factor C_X [31]. Therefore, the soft component is also multiplied by C_X to account for feeddown.

For the hard component, m_T scaling is used because the radial flow is assumed to be accounted for in the soft component. Because the hard component accounts for almost all of the yield at high momenta (see Fig. 5.1), the normalization of f_{hard} is multiplied by the m_T scaling factor which is the ratio X/π^0 for high p_T.

In short, the procedure to go from a measured π spectrum to the spectrum of another hadron X is:

$$\begin{aligned} f_{\text{hard}}(p_T) &\rightarrow C_X \, f_{\text{hard}}(\sqrt{p_T^2 + m_X^2 - m_\pi^2}) \\ f_{\text{soft}}(p_T; m_\pi) &\rightarrow A_X \, C_X \, f_{\text{soft}}(p_T; m_X) \end{aligned} \tag{5.3}$$

It is important to always check that the contribution of the soft component dominates at low p_T after fitting: if the hard component is too large at low momenta, it is questionable whether collective flow is necessary to describe the collision.

In Pb-Pb collisions at LHC and Au-Au collisions at RHIC, it is assumed that a radial flow is present [5]. Under this assumption, the soft component should contribute a significant fraction of the yield at low p_T. If it does not, a part of the spectrum with flow is attributed to the hard component that does not incorporate flow. In the extrapolation to other particles, the flow is therefore underestimated. In the case that the data is well described by the hard component without flow, this model reduces to m_T scaling since the part that contains all the flow is negligible. It is relatively arbitrary how large the hard component can be at low p_T before becoming problematic, which is a weakness of this model.

To get parameters that are compatible with the four particle species, a simultaneous fit to charged pions and kaons (from [23]) is done. The fit function is

$$\begin{aligned} f(p_T) = C_X \, (A_X \, f_{\text{soft}}(p_T; A, m_X, n, \beta_s, T) \\ + f_{\text{hard}}(p_T; A_1, p_1, n_1, A_2, p_2, n_2)) \end{aligned} \tag{5.4}$$

C_π was set to 1 since all particles are modified in reference to the pion yields and C_K is fixed to the ratio obtained in Chapter 3 from the data, $C_K = 0.485$, for faster fit convergence.

The result is plotted in Fig. 5.3. Aside from the very low p_T region below $0.5\,\mathrm{GeV}$, the fit describes the data well up to $8\,\mathrm{GeV}$ for both particles with the same set of parameters.

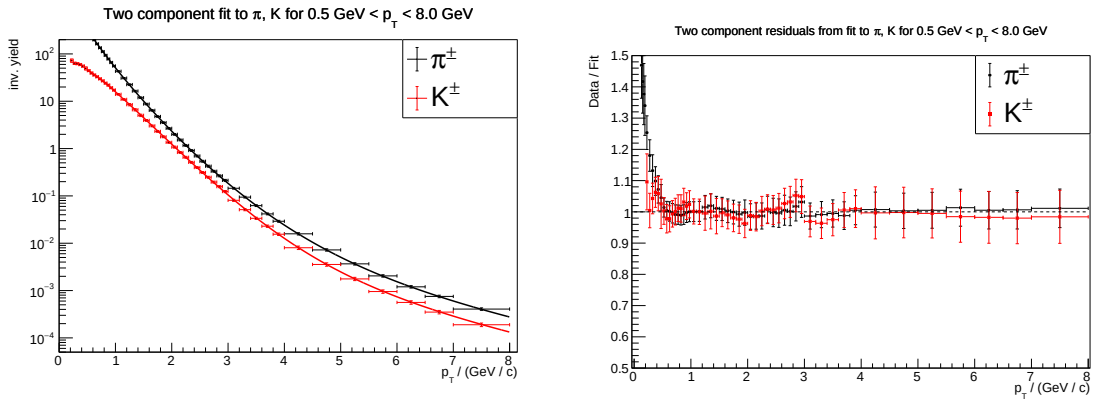

(a) Simultaneous fit of two-component model to $\pi^\pm$ and $K^\pm$ **(b)** Data / fit

Figure 5.3: Two component fit to charged $\pi^\pm$ and $K^\pm$

With the parameters from the fit, the invariant yield of the η meson and its ratio to the π^0 yield can be predicted. It is plotted together with the one from m_T scaling and the $K^\pm/\pi^\pm$ ratio parametrization in Fig. 5.4.

Because the two-component model describes the $\pi^\pm$ and the $K^\pm$ data very well, and the shape of the η spectrum is very similar to the K spectrum due to their similar masses, the η/π^0 ratio also shows a bump at around $2.5\,\mathrm{GeV}$.

Unlike the $K^\pm/\pi^\pm$ ratio, the two-component model can be used for the other relevant particles (ω, η') as well. The resulting ratios are multiplied by a constant so that the ratios are roughly equal at high p_T for comparison and plotted in Fig. 5.5. The plot shows that the peak that was seen in the $K^\pm/\pi^\pm$ ratio moves to higher momenta with increasing particle mass. One explanation is that heavier particles are more effected by flow than lighter particles in the blastwave model. The factor A_X from the statistical model is smaller for higher masses and supresses the soft component. The spectrum from the two-component model resembles m_T scaling more and more if the hard component dominates over the whole range. Therefore the bump becomes smaller for heavier particles: the highest point in the η'/π^0 ratio is only slightly above the constant value at high p_T.

5.2 Comparison With Data

To assess the validity of the predictions from this model, X/π^0 ratios can be predicted for particles other than pions and kaons. The data for mesons is rather sparse: there exist some measurements for η mesons [37, 38], but the results have much larger uncertainties than

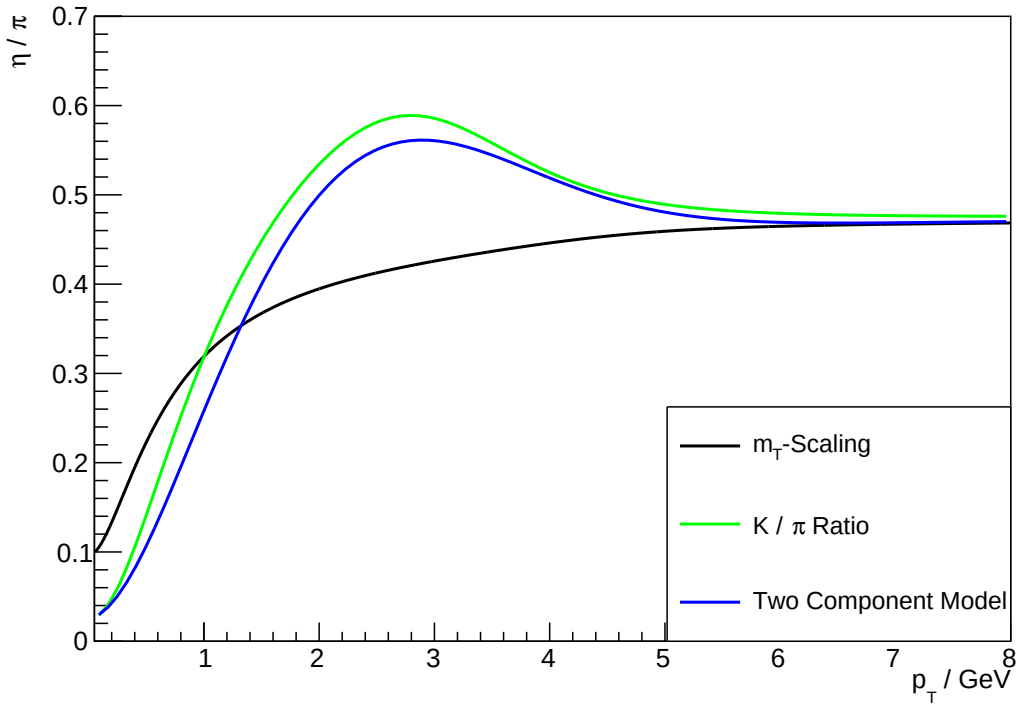

Figure 5.4: η/π^0 ratio from m_T scaling, $K^{\pm}/\pi^{\pm}$ ratio and two-component model

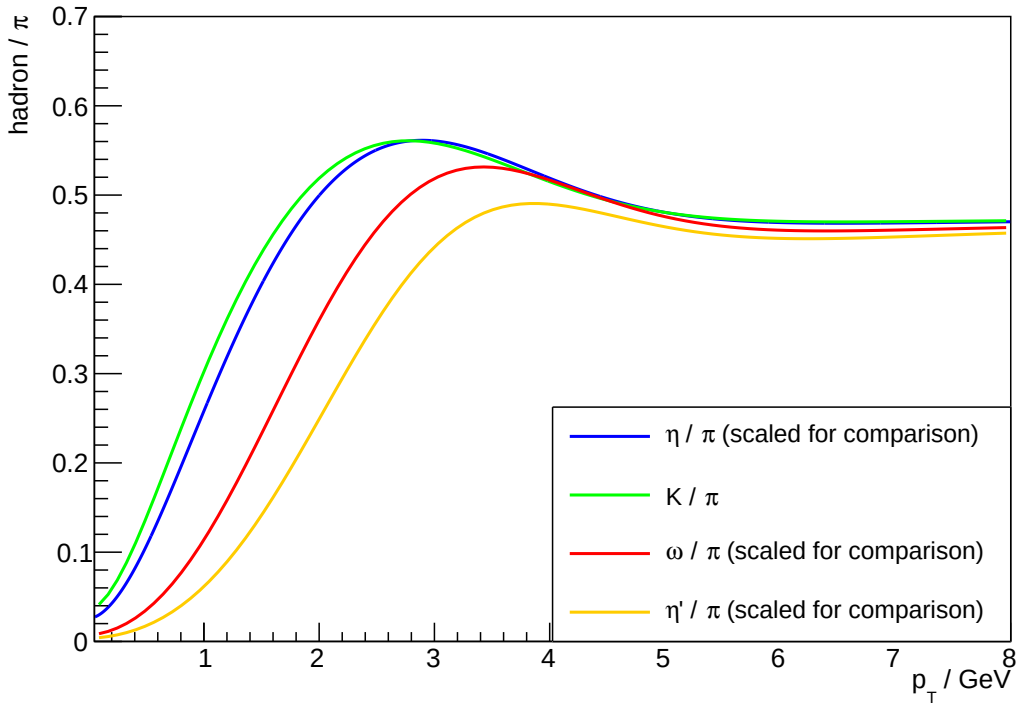

Figure 5.5: hadron $/\pi^0$ ratios for $K^{\pm}, \eta, \omega, \eta'$ from two-component model

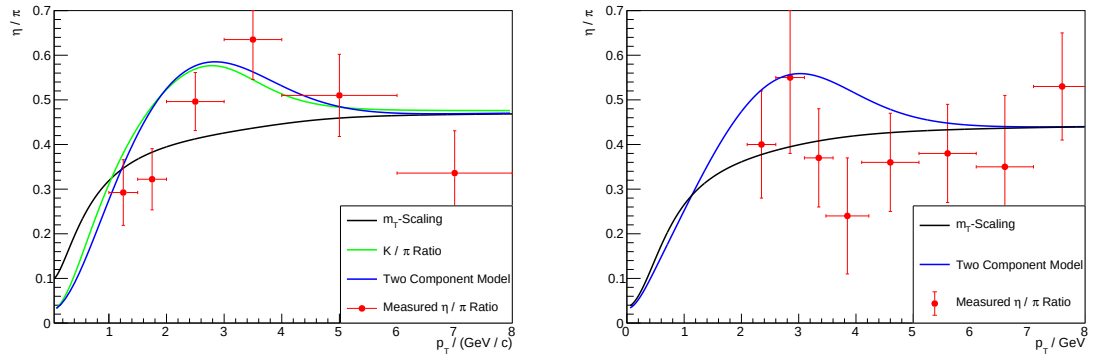

(a) **(b)**

Figure 5.6: η/π^0 ratios at a) ALICE [37] and b) PHENIX [26] with measurements

the ones for charged kaons and pions. The measurements at ALICE [37] are shown together with the prediction from m_T scaling and the two-component model in Fig. 5.6a.

They show no major disagreement with the prediction: they also show the bump at $3\,\mathrm{GeV}$ are sometimes larger and sometimes smaller than the prediction, which is expected if the errors are gaussian and the data follows the model. The measurements are described just as well by the measured $K^{\pm}/\pi^{\pm}$ ratio because the prediction for the η is very similar to the one for kaons.

The same procedure, i.e. the fit of the model to charged pion and kaon spectra was repeated with data from PHENIX at RHIC [26], which is also a heavy-ion collider experiment similar to ALICE. In the fit, the $K^{\pm}/\pi^{\pm}$ at high p_T was fixed to aid the fit convergence because there were no $K^{\pm}$ measurements above $4\,\mathrm{GeV}$. Fig. 5.6b shows the measurements in Au-Au collisions from PHENIX with the prediction from the two-component model and m_T scaling.

Here, m_T scaling describes the data well, as the PHENIX collaboration already noticed [26]. The two-component model, which includes radial flow in the soft component, is a worse description of the data. This looks like there is no radial or little radial flow for η mesons at PHENIX and calls into question whether such a model with collective radial flow is needed to describe the data at PHENIX. On the other hand, the creation of the QGP at RHIC [39] and its expansion would suggest that radial flow is present in the collisions and would have to be factored in for any fit to the data.

5.3 Cocktail Simulation for Pb-Pb at ALICE

The cocktail simulation is repeated with the hadron/π^0 ratios for Pb-Pb collisions with a center-of-mass energy $\sqrt{s_{\mathrm{NN}}} = 2.76\,\mathrm{TeV}$ at ALICE. The photon yields divided by the reference yields are shown in Fig. 5.7. The η, ω and η' yields are now higher as expected from Fig. 5.5. Separately, they increase from η, ω and η' increase to up to 1.3 times the yields from

m_T scaling. With increasing mass, the peak moves to higher momenta as indicated in Fig. 5.5.

At very low p_T, the decay-photon spectrum is smaller than the one from m_T scaling. This can be interpreted as the photons being boosted from low p_T to higher momenta in the collective flow.

Because the ω and η' mesons contribute much less to the decay-photon yield than the η meson (Fig. 2.2), most of the increase in overall decay-photons in Fig. 5.7b comes from the change of the η/π^0 ratio. The decay-photon yield goes up to ≈1.05 times the yield from m_T scaling which is similar to the result from the $K^{\pm}/\pi^{\pm}$ ratio. The direct photon yield therefore also decreases by about 30% in this model.

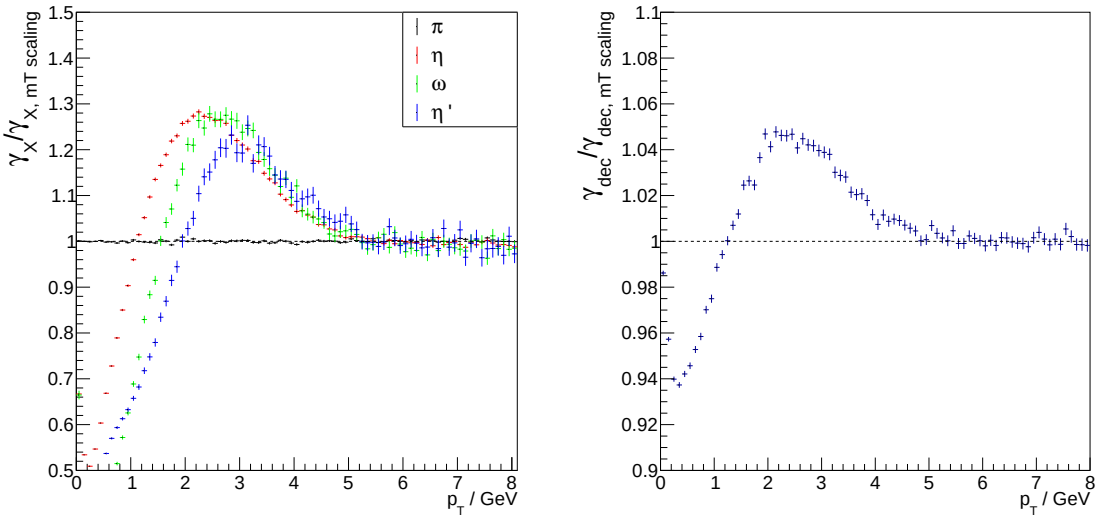

(a) **(b)**

Figure 5.7: Change of decay-photon yield $\frac{\gamma_{\mathrm{dec,\,new}}}{\gamma_{\mathrm{dec},\,m_T\,\mathrm{scaling}}}$ for two-component model. (a) by particle species, (b) in total

5.4 Cocktail Simulation for Au-Au at PHENIX

Regardless of the discrepancy between the η/π^0 ratio from measurements and the model, the same procedure using the two-component model is now applied to the measurements in Au+Au collisions with a center-of-mass energy of $\sqrt{s_{\mathrm{NN}}} = 200\,\mathrm{GeV}$ at PHENIX although the results are likely not realistic because the η/π^0 ratio is well described by m_T scaling. It is particularly interesting to compare the results from this model to the published ones because firstly, only m_T scaling was used which makes the comparison straightforward and secondly, the direct photon flow puzzle (see Chapter 1.4) and the discrepancy between the results from STAR and PHENIX (Fig. 1.3) indicate that the direct photon yield at RHIC is not completely understood [18].

First, the parameters for the soft and hard components are obtained by a simultaneous fit to $K^{\pm}$ and $\pi^{\pm}$ spectra from [40]. The fit is shown in Fig. 5.8 and the parameters are in Appendix 7.2. The extrapolation to other particle ratios is shown in Fig. 5.9. The peaks in the hadron/π^0 ratios are now higher: the η/π^0 ratio goes up to 0.6 whereas the highest point in the calculation for Pb-Pb is at approximately 0.55. In addition to this, the peaks of the heavier particles are more pronounced than in the Pb-Pb calculation. The reason for this is that in the PHENIX measurements, the invariant yield declines much more steeply for increasing momentum. If now 1% of particles are boosted up in momentum from p_0 by some momentum Δp, the boosted particles make up a large fraction of all particles at $p_0 + \Delta p$. Therefore the X/π^0 ratio increases more than at ALICE.

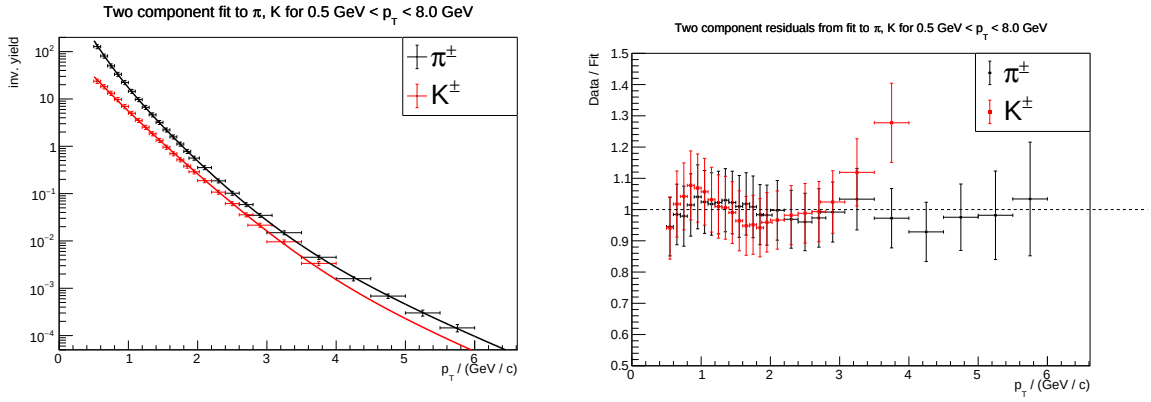

(a) Simultaneous fit of two-component model to $\pi^{\pm}$ and $K^{\pm}$ **(b)** Data / fit

Figure 5.8: Two component fit to charged $\pi^{\pm}$ and $K^{\pm}$ from PHENIX [40]

This is also reflected in the change of the decay-photon yield for PHENIX shown in Fig. 5.10. It increases by 7% compared to m_T scaling in this model. The R_γ published by the PHENIX collaboration in Ref. [3] is shown in Fig. 5.11. It is ≈1.3 in the range between $1\,\mathrm{GeV}$ and $4\,\mathrm{GeV}$ for 0-20% centrality which is much larger than at ALICE (Fig. 3.3). At $3\,\mathrm{GeV}$, R_γ would decrease to ≈1.2, which means that about a third of the direct photon signal could be attributed to decay-photons in this model.

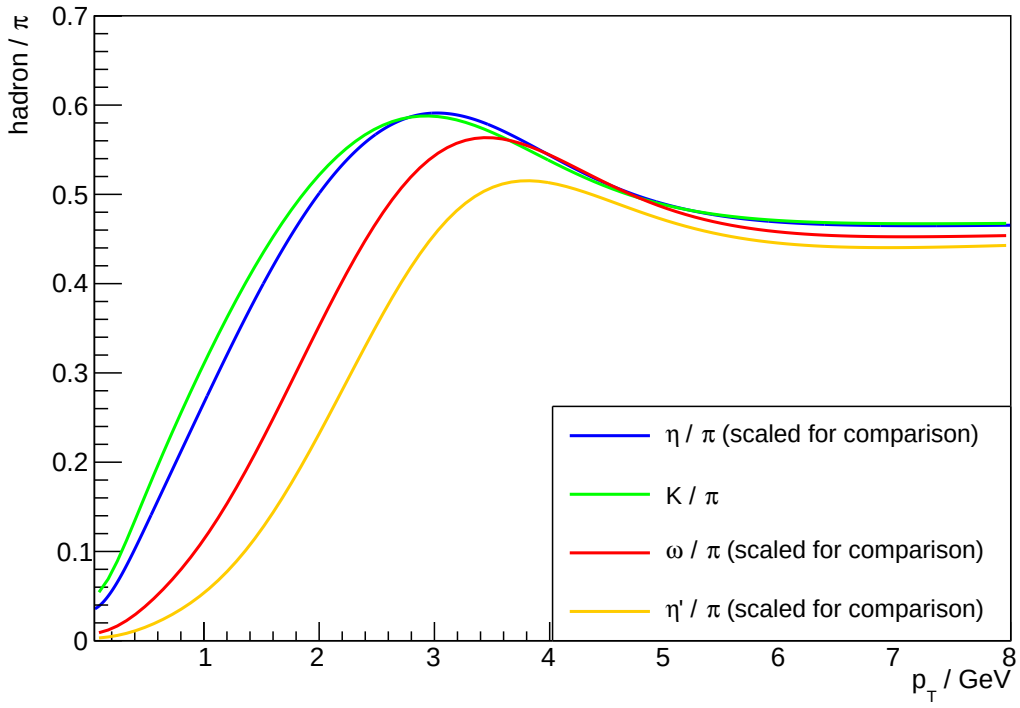

Figure 5.9: hadron $/\pi^0$ ratios for different $K^{\pm}, \eta, \omega, \eta'$ from two-component model for PHENIX data

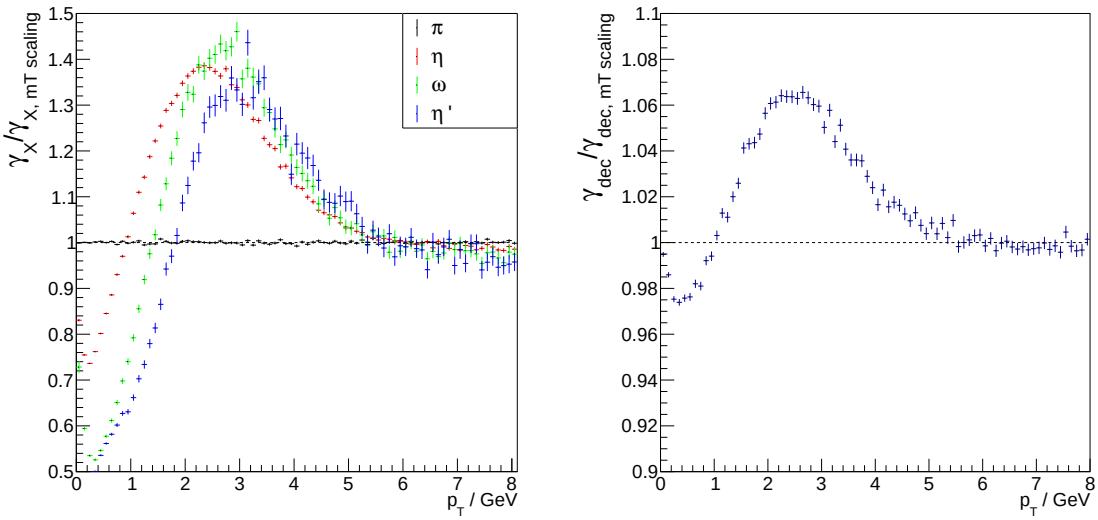

(a) **(b)**

Figure 5.10: Change of decay-photon yield $\frac{\gamma_{\mathrm{dec,\,new}}}{\gamma_{\mathrm{dec},\,m_T\,\mathrm{scaling}}}$ for two-component model for PHENIX. (a) by particle species, (b) in total

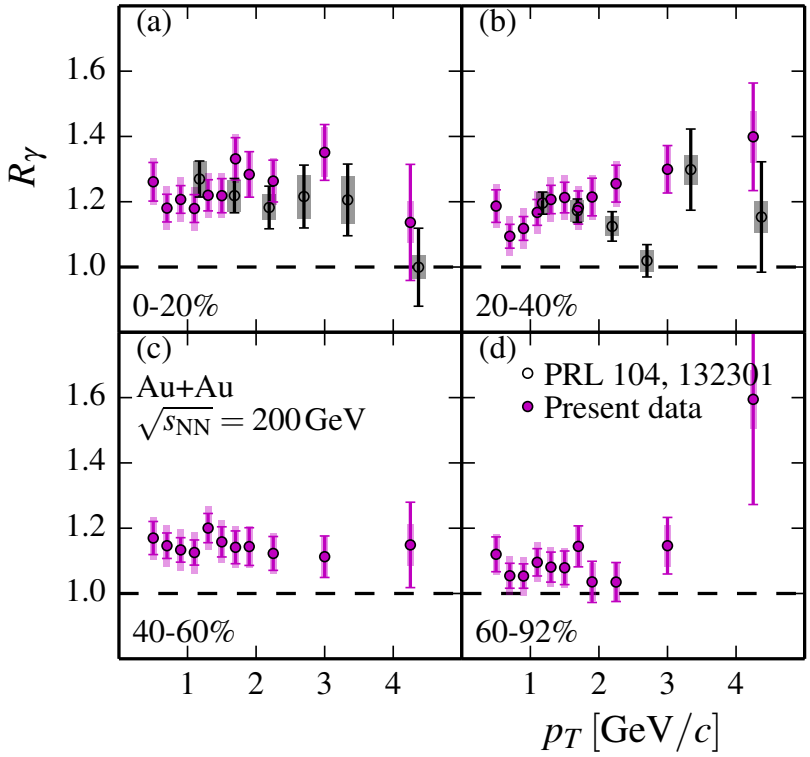

Figure 5.11: R_γ from PHENIX [3]

Summary and Discussion

6

Four different methods for predicting unknown particle yields in Pb-Pb collisions are compared: m_T scaling, taking the $K^{\pm}/\pi^{\pm}$ ratio as an approximation for the η/π^0 ratio, Tsallis-blastwave fits and a two-component model. The fit from the Tsallis-blastwave model does not describe the known charged pion and kaon yield and is not usable for extrapolation to other particles.

Because kaons have masses similar to η mesons, it is assumed that they are similarly affected by collective radial flow and the η/π^0 is substituted by $K^{\pm}/\pi^{\pm}$. The K^0_S, which also has a similar mass, was already used in cocktail calculations at ALICE [2] although the authors took the average of m_T scaling and the ratio from K^0_S as the η/π^0 ratio. Radial flow was therefore already partly incorporated. When comparing the $K^{\pm}/\pi^{\pm}$ and the $K^0_S/\pi^{\pm}$ ratios, the ratio with charged kaons show a larger peak than the ratio with neutral kaons even though the masses of $K^{\pm}$ and K^0_S are almost identical. The reason for this difference is unclear, but this means that in the cocktail calculation in Ref. [2] fewer η mesons were decayed than if the $K^{\pm}/\pi^{\pm}$ had been used. Compared to m_T scaling, the $K^{\pm}/\pi^{\pm}$ ratio is up to ≈40% larger between $1\,\mathrm{GeV}$ and and $5\,\mathrm{GeV}$. After accounting for the averaging and the difference between K^0_S and $K^{\pm}$, this translates to an increase of the decay photon yield by up to 5% at about $\approx 2\,\mathrm{GeV}$. Almost a third of direct photons at this momentum could be attributed to decay-photons instead of direct photons. This method works well for the η meson because it is simple and matches the measured η/π^0 ratio reasonably well. The severe limitation is that this can only be applied to the η because all other particles have masses that differ by a lot from the one of charged kaons. For the ω and η', another approach is necessary.

In the two-component model, the spectrum of charged pions and kaons is fit with the sum of a blastwave component for low p_T and two Hagedorn type terms for high p_T. To predict the η, ω and η' spectra, the mass and normalization in the soft component are changed and m_T scaling is done in the hard component. The fit describes the charged pion and kaon spectra well and the prediction for the η spectrum shows no major disagreement with measurements at ALICE. The prediction for η from this model is very close to the measured $K^{\pm}/\pi^{\pm}$ ratio. For heavier mesons, the boost due to radial flow is larger and the peak in the ratio to π^0 moves to higher p_T while the ratio decreases at low p_T. With the contributions from η, ω and η', the decay photon yield goes up by a factor up to ≈1.07 at $2\,\mathrm{GeV}$ in this model. Here, also a third of previously assigned direct photons would now be attributed to decay-photons at this momentum if this decay-photon calculation was used. These two results show that even a difference by a few percent in the decay-photon cocktail can drastically change the direct photon measurements.

The η/π^0 ratio from the two-component model was very close to the $K^{\pm}/\pi^{\pm}$ ratio, which was expected due to the similar masses. For the η meson, this model is therefore very similar to the first one. The strength of this approach is that it can also be used for ω and η' mesons, although assessing the accuracy of these predictions is difficult due to very few measurements.

A complete cocktail simulation requires baryons such as the Σ^0 in addition to mesons. Because baryons and fermions have different m_T spectra, a new set of parameters would be necessary because their m_T spectra are different. Since very heavy particles firstly only contribute a small fraction of the decay photon cocktail, a change in the predicted momentum distribution of particles other than the four mesons discussed in this thesis gives an almost identical decay-photon spectrum. One should therefore concentrate on the lighter particles, which contribute the most photons.

One drawback is that it is not clear to what extent the hard component contributes at very low p_T. Conceptually, one would expect that the low p_T region is dominated by the soft component with radial flow in heavy-ion collisions. When comparing the prediction with the η measurements from PHENIX, it looks like there is almost no flow and the hard component makes up most of the spectrum.

Nonetheless, I think that the two-component model is better suited for decay photon calculations than m_T scaling and the substitution by $K^{\pm}/\pi^{\pm}$. It reduces to m_T scaling if the data shows no radial flow. The η/π^0 ratio from the two-component model is similar to the $K^{\pm}/\pi^{\pm}$ because the modification due to the mass difference is small. This modification based on theory and previous observations likely improves the prediction.

One possible improvement would be to incorporate the effect of feeddown in the soft component. Currently, feeddown is taken to be independent of the transverse momentum. A feeddown simulation could be done with many particle species following e.g. the blastwave model. With the fraction of primary and secondary particles from this simulation, the soft component could be corrected to also include the feeddown products.

Appendix

7

7.1 Blastwave normalization

The derivation of the normalization is partly shown in [41]: in a grand canonical ensemble, the logarithm of the partition function for particle species i is given by

$$\ln Z_i = \frac{V g_i}{2\pi^2} \int_0^\infty \pm p^2 \, \mathrm{d}p \ln \left(1 \pm \exp\left(-\frac{E_i - \mu_i}{T_{\mathrm{chem}}}\right)\right) \tag{7.1}$$

with the volume V, the chemical freeze-out temperature T_{chem}, the spin degeneracy $g_i = 2J + 1$, the energy $E_i = \sqrt{p_i^2 + m_i^2}$ and '+' for fermions, '-' for bosons. The particle density for species i is then

$$\begin{aligned} N_i &= -\frac{T_{\mathrm{chem}}}{V} \frac{\partial \ln Z_i}{\partial \mu_i} \\ &= \frac{g_i}{2\pi} \int_0^\infty \frac{p^2 \, \mathrm{d}p}{\exp\left(E_i - \mu_i\right)/T_{\mathrm{chem}} \pm 1} \\ &= \frac{g_i}{2\pi^2} m_i^2 T_{\mathrm{chem}} \sum_{k=1}^{\infty} \frac{\mp 1^{k+1}}{k} \left(e^{\mu_i / T_{\mathrm{chem}}}\right)^k K_2\left(\frac{k m_i}{T_{\mathrm{chem}}}\right) \\ &\approx \frac{g_i}{2\pi^2} m_i^2 T_{\mathrm{chem}} K_2\left(m_i / T_{\mathrm{chem}}\right) \quad \text{with } k > 1 \text{ terms neglected and } \mu_i \approx 0 \end{aligned} \tag{7.2}$$

The ratio of two particle densities N_i and N_j is then

$$\frac{N_i}{N_j} \approx \frac{m_i^2 K_2(m_i/T_{\mathrm{chem}})}{m_j^2 K_2(m_j/T_{\mathrm{chem}})} \tag{7.3}$$

On the other hand, the particle density is given by

$$\frac{N_X}{V} = \frac{1}{V} \iiint \mathrm{d}\phi \, \mathrm{d}y \, p_T \, \mathrm{d}p_T \frac{\mathrm{d}^3 n_X}{\mathrm{d}\phi \, \mathrm{d}y \, p_T \, \mathrm{d}p_T} \tag{7.4}$$

$$= \frac{2\pi}{V} \iint \mathrm{d}y \, p_T \, \mathrm{d}p_T \frac{\mathrm{d}^2 n}{\mathrm{d}y \, p_T \, \mathrm{d}p_T} \tag{7.5}$$

In collisions, the fireball not only expands radially, but also longitudinally. This can be taken into account by splitting up the hot region into small sources i that are boosted in the z-direction by some rapidity Δy_i. If $g(y)$ is the rapidity distribution of a stationary source,

then the distribution in the lab-frame is $g(y + \Delta y_i)$ since a Lorentz boost only changes the rapidity by a constant. The detector at mid-rapidity only recieves the particles with $y = 0$. With $0 = y + \Delta y_i$, contribution of the boosted source is proportional to $g(-\Delta y_i)$. In the limit of infinitesimally small sources, this is equivalent to integrating over the rapidity distribution g(Δy).

Therefore the ratio of particles at mid-rapidity should be the same as the one that is obtained by integrating over the whole rapidity range:

$$\left.\frac{N_X}{N_\pi}\right|_{y=0} = \frac{\iint \mathrm{d}y\ p_T\,\mathrm{d}p_T\ \dfrac{\mathrm{d}^2N_X}{\mathrm{d}y\ p_T\,\mathrm{d}p_T}}{\iint \mathrm{d}y\ p_T\,\mathrm{d}p_T\ \dfrac{\mathrm{d}^2N_\pi}{\mathrm{d}y\ p_T\,\mathrm{d}p_T}} \tag{7.6}$$

A factor A_X is introduced to include the change in the normalization. The soft component of a particle X is then $A_X \cdot f^X(p_T)$. One can work out that integrating over the soft component gives

$$\int p_T f^X(p_T)\,\mathrm{d}p_T \propto m_X^2 K_2(m_X/T_{\mathrm{kin}}) \tag{7.7}$$

where T_{kin} is the temperature parameter in the blastwave model. Equations 7.3, 7.6 and 7.7 together then result in

$$\left.\frac{N_X}{N_\pi}\right|_{y=0} = \frac{N_X}{N_\pi} = \frac{\iint \mathrm{d}y\ p_T\,\mathrm{d}p_T\ \dfrac{\mathrm{d}^2N_X}{\mathrm{d}y\ p_T\,\mathrm{d}p_T}}{\iint \mathrm{d}y\ p_T\,\mathrm{d}p_T\ \dfrac{\mathrm{d}^2N_\pi}{\mathrm{d}y\ p_T\,\mathrm{d}p_T}} \tag{7.8}$$

$$\approx A_X \frac{m_X^2 K_2(m_X/T_{\mathrm{kin}})}{m_\pi^2 K_2(m_\pi/T_{\mathrm{kin}})} \tag{7.9}$$

$$\stackrel{!}{=} \frac{m_X^2 K_2(m_X/T_{\mathrm{chem}})}{m_\pi^2 K_2(m_\pi/T_{\mathrm{chem}})} \tag{7.10}$$

Then A_X is given by

$$A_X = \frac{n_X}{n_\pi} \approx \frac{m_\pi^2 K_2(m_\pi/T_{\mathrm{kin}})}{m_X^2 K_2(m_X/T_{\mathrm{kin}})} \frac{m_X^2 K_2(m_X/T_{\mathrm{chem}})}{m_\pi^2 K_2(m_\pi/T_{\mathrm{chem}})} \tag{7.11}$$

7.2 Fit results

π^0 parametrization

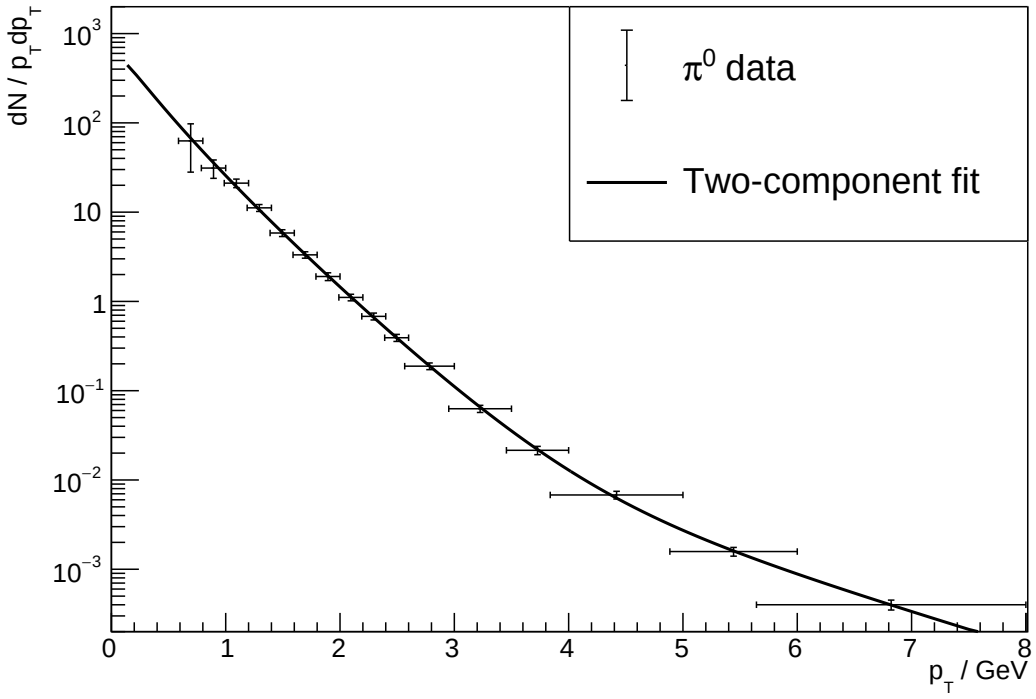

Figure 7.1: Parametrization of π^0 spectrum with fit from two component model

Table 7.1: Parameters of fit in Fig. 7.1

C_X	1
A	1.757e+04
β_S	7.891e-01
T	1.500e-01
n	7.120e-01
A_1	3.180e-01
p_1	4.550e+01
n_1	4.796e+01
A_2	0
p_2	-
n_2	-

Here, the fit worked well enough without the second term in Eq.(5.1). A_2 was fixed to zero eliminating that term.

$K^{\pm}/\pi^{\pm}$ parametrization

The fit function is

$$\frac{K^{\pm}}{\pi^{\pm}}(p_T) = N_1 \frac{\exp\left(\frac{\beta p_T - \sqrt{p_T^2+m_K^2}}{T_{\rm kin}\sqrt{1-\beta^2}}\right) + C_K N_2 \left(1+\frac{p_T^2}{p_0^2}\right)^{-n}}{\exp\left(\frac{\beta p_T - \sqrt{p_T^2+m_\pi^2}}{T_{\rm kin}\sqrt{1-\beta^2}}\right) + N_2 \left(1+\frac{p_T^2}{p_0^2}\right)^{-n}}. \tag{7.12}$$

The result of the fit were the parameters:

Table 7.2: Parameters of fit in Fig. 3.1

N_1	0.991
β	0.904
T_{kin}	0.176
C_K	0.497
N_2	2.08e+05
p_0	0.218
n	-1.203

Tsallis-Blastwave parameters

Table 7.3: Parameters of fit in Fig. 3.1

q	1.062
T	0.109
β	0.454

Two-component parameters for ALICE

Table 7.4: Parameters of fit to ALICE invariant yields in Fig. 5.3

A	1.76e+5
β	0.878
T	0.094
n	0.760
A_1	0.665
p_1	5.667
n_1	8.940
A_2	139.2
p_2	8.034
n_2	22.50

Two-component parameters for PHENIX

Table 7.5: Parameters of fit to PHENIX invariant yields in Fig. 5.8

A	1.01e+4
β	0.885
T	0.108
n	0.796
A_1	1.290
p_1	9.862
n_1	20.0
A_2	1566.9
p_2	5.875
n_2	30.0

Bibliography

[1] Rupa Chatterjee, Lusaka Bhattacharya, and Dinesh K. Srivastava. „Electromagnetic Probes“. In: *The Physics of the Quark-Gluon Plasma: Introductory Lectures*. Ed. by Sourav Sarkar, Helmut Satz, and Bikash Sinha. Berlin, Heidelberg: Springer Berlin Heidelberg, 2010, pp. 219–264.

[2] Jaroslav Adam et al. „Direct Photon Production in Pb-Pb Collisions at $\sqrt{s_{NN}} = 2.76$ TeV“. In: *Phys. Lett.* B754 (2016), pp. 235–248.

[3] A. Adare et al. „Centrality Dependence of Low-Momentum Direct-Photon Production in Au$+$Au Collisions at $\sqrt{s_{NN}} = 200$ GeV“. In: *Phys. Rev.* C91.6 (2015), p. 064904.

[4] STAR Collaboration. „Direct Virtual Photon Production in Au+Au Collisions at $\sqrt{s_{NN}} = 200$ GeV“. In: (2016). arXiv: 1607.01447.

[5] Michael Kliemant et al. „Global Properties of NucleusNucleus Collisions“. In: *The Physics of the Quark-Gluon Plasma*. Lecture Notes in Physics. Springer, Berlin, Heidelberg, 2009, pp. 23–103.

[6] Heng-Tong Ding, Frithjof Karsch, and Swagato Mukherjee. „Thermodynamics of Strong-Interaction Matter from Lattice QCD“. In: (). arXiv: 1504.05274.

[7] P.D. Hermes et al. „Measured and Simulated Heavy-Ion Beam Loss Patterns at the CERN Large Hadron Collider“. In: *Nuclear Instruments and Methods in Physics Research Section A: Accelerators, Spectrometers, Detectors and Associated Equipment* 819 (May 2016), pp. 73–83.

[8] Y. Cheng et al. „Transverse Expansion in $^{197}\mathrm{Au} + {}^{197}\mathrm{Au}$ Collisions at RHIC“. In: *Physical Review C* 68.3 (Sept. 18, 2003), p. 034910.

[9] C.Y. Wong. *Introduction to High-Energy Heavy-Ion Collisions*. Introduction to High-energy Heavy-ion Collisions. World Scientific, 1994.

[10] J. Stachel et al. „Confronting LHC Data with the Statistical Hadronization Model“. In: *Journal of Physics: Conference Series* 509 (May 7, 2014), p. 012019. arXiv: 1311.4662.

[11] Tetsufumi Hirano, Naomi van der Kolk, and Ante Bilandzic. „Hydrodynamics and Flow“. In: *The Physics of the Quark-Gluon Plasma: Introductory Lectures*. Ed. by Sourav Sarkar, Helmut Satz, and Bikash Sinha. Berlin, Heidelberg: Springer Berlin Heidelberg, 2010, pp. 139–178.

[12] Tapan K. Nayak. „Heavy Ions: Results from the Large Hadron Collider“. In: *Pramana* 79.4 (Oct. 2012), pp. 719–735. arXiv: 1201.4264.

[13] The ALICE Collaboration et al. „The ALICE Experiment at the CERN LHC“. In: *Journal of Instrumentation* 3 (08 2008), S08002.

[14] *The Large Hadron Collider*. URL: https://home.cern/topics/large-hadron-collider.

[15] *CERN | Accelerating Science*. URL: https://home.cern/.

[16] Helmut Satz. „The Thermodynamics of Quarks and Gluons“. In: *The Physics of the Quark-Gluon Plasma: Introductory Lectures*. Berlin, Heidelberg: Springer Berlin Heidelberg, 2010, pp. 1–21.

[17] Rupa Chatterjee, Lusaka Bhattacharya, and Dinesh K. Srivastava. „Electromagnetic Probes“. In: *The Physics of the Quark-Gluon Plasma*. Lecture Notes in Physics. Springer, Berlin, Heidelberg, 2009, pp. 219–264.

[18] Charles Gale. „Direct Photon Production in Relativistic Heavy-Ion Collisions – a Theory Update“. In: (2018). arXiv: 1802.00128.

[19] Martin Rudolf Wilde. „Measurement of Direct Photons in Pp and PbPb Collisions with Conversion Pairs“. PhD Thesis. Westfälischen Wilhelms-Universität Münster, 2015.

[20] Jean-François Paquet et al. „The Production of Photons in Relativistic Heavy-Ion Collisions“. In: *Physical Review C* 93.4 (Apr. 18, 2016). arXiv: 1509.06738.

[21] M. Deutschmann et al. „Transverse Spectra in $\pi^{\pm}$p and Kp Interactions between 8 and 16 GeV/c“. In: *Nuclear Physics B* 70.2 (Feb. 25, 1974), pp. 189–204.

[22] J. Bartke et al. „Simplicity of Transverse Energy Spectra of Hadrons“. In: *Nuclear Physics B* 120.1 (Mar. 7, 1977), pp. 14–22.

[23] Jaroslav Adam et al. „Centrality Dependence of the Nuclear Modification Factor of Charged Pions, Kaons, and Protons in Pb-Pb Collisions at $\sqrt{s_{NN}}$ = 2.76 TeV“. In: *Phys. Rev.* C93.3 (2016), p. 034913.

[24] Richard Witt and for the STAR Collaboration. „Systematics and Mt-Scaling“. In: (Mar. 12, 2004). arXiv: nucl-ex/0403021.

[25] Ekkard Schnedermann, Josef Sollfrank, and Ulrich Heinz. „Thermal Phenomenology of Hadrons from 200A GeV S+S Collisions“. In: *Physical Review C* 48.5 (1993), p. 2462.

[26] PHENIX Collaboration and S. S. Adler. „High Transverse Momentum Eta Meson Production in p+p, d+Au and Au+Au Collisions at $\sqrt{s_{NN}}$ = 200 GeV“. In: *Physical Review C* 75.2 (Feb. 27, 2007), p. 26. arXiv: nucl-ex/0611006.

[27] Kun Jiang et al. „Onset of Radial Flow in p+p Collisions“. In: *Phys. Rev.* C91.2 (2015), p. 024910.

[28] Zebo Tang et al. „Spectra and Radial Flow at RHIC with Tsallis Statistics in a Blast-Wave Description“. In: *Phys.Rev.C79:051901,2009* (Dec. 9, 2008). arXiv: 0812.1609.

[29] Betty Bezverkhny Abelev et al. „Neutral Pion Production at Midrapidity in pp and Pb-Pb Collisions at $\sqrt{s_{NN}}$ = 2.76 TeV“. In: *Eur. Phys. J.* C74.10 (2014), p. 3108.

[30] Rene Brun and Fons Rademakers. *ROOT - An Object Oriented Data Analysis Framework*.

[31] Klaus Reygers. personal communication. 2017.

[32] Torbjörn Sjöstrand, Stephen. Mrenna, and Peter Skands. *PYTHIA8, JHEP05 (2006) 026, Comput. Phys. Comm. 178 (2008) 852*.

[33] A. Adare et al. „Neutral Pion Production with Respect to Centrality and Reaction Plane in Au+Au Collisions at $\sqrt{s_{NN}}$ = 200 GeV“. In: *Physical Review C* 87.3 (Mar. 28, 2013). arXiv: 1208.2254.

[34] C. Patrignani et al. „Review of Particle Physics“. In: *Chin. Phys.* C40.10 (2016), p. 100001.

[35] Betty Bezverkhny Abelev et al. „K^0_S and Production in Pb-Pb Collisions at $\sqrt{s_{NN}}$ = 2.76 TeV“. In: *Phys. Rev. Lett.* 111 (2013), p. 222301.

[36] U. Heinz and G. Kestin. „Jozsó's Legacy: Chemical and Kinetic Freeze-out in Heavy-Ion Collisions“. In: *The European Physical Journal Special Topics* 155.1 (Mar. 2008), pp. 75–87.

[37] Lucia Leardini. „Measurement of Neutral Mesons and Direct Photons in in Pb-Pb Collisions at sNN= 2.76 TeV with the ALICE Experiment at the LHC“. 2017.

[38] P. K. Khandai, P. Shukla, and V. Singh. „Meson Spectra and M_T Scaling in p+p, d+Au and Au+Au Collisions at $\sqrt{s_{NN}}$ = 200 GeV“. In: *Physical Review C* 84.5 (). arXiv: 1110.3929.

[39] STAR Collaboration and J. Adams. „Experimental and Theoretical Challenges in the Search for the Quark Gluon Plasma: The STAR Collaboration's Critical Assessment of the Evidence from RHIC Collisions“. In: (Jan. 13, 2005). arXiv: nucl-ex/0501009.

[40] A. Adare et al. „Spectra and Ratios of Identified Particles in Au+Au and d+Au Collisions at $\sqrt{s_{NN}}$ = 200 GeV“. In: *Phys. Rev.* C88.2 (2013), p. 024906.

[41] Klaus Reygers. „Quark Gluon Plasma Physics: 5. Statistical Model and Strangeness“. 2017.